Acta Geotechnica (2006) 1:107–122
DOI 10.1007/s11440-006-0012-x

RESEARCH PAPER

Conditions for instabilities in collapsible solids including volume implosion and compaction banding

Ronaldo I. Borja

Received: 26 November 2005 / Revised: 29 March 2006 / Accepted: 23 May 2006 / Published online: 22 August 2006

Abstract We review conditions for material instabilities in porous solids induced by a bifurcation of solution into non-unique strain rate fields. Bifurcation modes considered include jumps in the strain rate tensor of ranks one and higher representing deformation band and diffuse instability modes, respectively. Eigenmodes (e-modes) are extracted for each type of instability to fully characterize various frameworks of deformation in collapsible solids. For diffuse instability these e-modes are determined from a homogeneous system of linear equations emanating from the condition of zero jump in the stress rate tensor, which in turn demands that the tangent constitutive tensor be singular for the existence of nontrivial solutions. For isotropic materials we describe two types of singularity of the constitutive tensor: (a) singularity of the constitutive matrix in principal axes, and (b) singularity of spin. Accordingly, we derive the e-modes for each type of singularity. We utilize the singularity of the constitutive matrix in principal axes as a precursor to volume implosion in collapsible solids such as loose sands undergoing liquefaction instability and high-porosity rocks undergoing cataclastic flow. Finally, we compare conditions and e-modes for volume implosion and compaction banding, two similar failure modes ubiquitous in granular soils and rocks.

Supported by U.S. Department of Energy, Grant DE-FG02-03ER15454, and U.S. National Science Foundation, Grants CMS-0201317 and CMS-0324674.

R. I. Borja (✉)
Department of Civil and Environmental Engineering,
Stanford University, Stanford, CA 94305, USA
e-mail: borja@stanford.edu

Keywords Compaction band · Deformation band · Material instability · Volume implosion

1 Introduction

Material instabilities in solids occur in a number of applications and in a variety of forms. Examples include Lüders bands in metals, cracking in concrete, microbuckling in cellular materials, kinking failure in fiber composites, stress-induced transformation in shape memory alloys, and shear strain localization in bulk metallic glasses. Geomaterials are also susceptible to ''unstable'' behaviors manifesting through compaction and dilation banding in rocks, shear banding in sands and clays, liquefaction of saturated loose sands, sanding in poorly cemented sandstones, and volume collapse in high-porosity unconsolidated sediments [1, 21, 24, 33, 43]. Such behaviors are governed by a nonlinear interaction of geometry and material properties and are best addressed from a micromechanical standpoint. However, a microstructural approach is not always feasible especially when these behaviors are to be predicted in a large-scale structure where typically only a macroscopic material model is available to make a prediction.

Strain localization in the form of shear bands has received enormous attention over the years, which is understandable because their appearance is ubiquitous in many natural and engineered materials. In soils and rocks strain localization is often used synonymously with terms such as ''slip surface'' and ''failure shear zone'' because of the appearance of significant shear offset. However, the term ''deformation band'' seems more general since a localized zone may also exhibit

significant pore growth (dilation) or pore collapse (compaction) appearing either alone or in combination with some shear offset [1, 2, 9, 10]. Prediction of the occurrence of deformation bands from a macroscopic material model is now well understood. In the framework of rate-independent elastoplasticity, one simply tracks the loss of ellipticity of the governing velocity equation of equilibrium to identify the onset of a deformation band. The procedure not only yields the orientation of the band but also determines the corresponding eigenmode (or e-mode) representing the type of deformation band formed, i.e., whether it is a dilation, compaction, shear, or a mixed-mode band.

In this paper, we develop a more general framework of instability analysis for collapsible solids based on a macroscale approach. The term ''collapsible'' generally refers herein to any weakly bonded high-porosity material, although we are more interested in collapsible geomaterials such as aeolian sands, underconsolidated sandstones, poorly cemented coquina, diatomite, and chalk. Such materials can exhibit an ''unstable'' behavior even though it may not lead to a deformation band. We shall call such material instability not associated with a deformation band as ''diffuse,'' even if this term is also used in a different context by other authors to mean ''global bifurcation,'' see [16]. For example, liquefaction of saturated loose sands occurs in a diffuse mode characterized by pore collapse where the volume implodes in all three spatial directions. Of course, pore collapse can also occur in one dimension along a narrow band, as exemplified by compaction banding in porous rocks where the volume simply compacts in the direction normal to the band [22, 33–35]. It appears, however, that a more general framework of failure modes is in order since one mode could conceivably trigger the other. An example of where this scenario could happen is when an unconsolidated sandstone undergoes pore collapse in front of a wellbore resulting in sand production and conceivably triggering a more widespread localized deformation pattern around the wellbore [21, 28, 29].

The theoretical underpinning of the proposed framework is the classical bifurcation theory in which we investigate local bifurcation modes characterized by jumps in the strain rate tensor of ranks one and higher [3, 4, 7, 15, 19, 27, 32, 41] representing deformation band and diffuse modes, respectively. For the constitutive description of the material we review conditions for the occurrence of such strain rate jumps in elastoplastic solids with associative and non-associative plastic flow along with softening plasticity. We recall the aspect of incremental nonlinearity and the role that comparison solids play in the analysis, particularly for materials exhibiting non-associative plastic flow. The paper highlights the appropriate e-modes for various modes of bifurcation, including that associated with volume implosion in all three spatial directions. Finally, we illustrate the framework with numerical stress-point calculations utilizing a class of three-invariant non-associative plasticity models to illustrate an interesting and important interplay among the various failure modes in a geomaterial.

As for notations and symbols, bold-faced letters denote tensors and vectors; the symbol '$\cdot$' denotes an inner product of two vectors (e.g. $\boldsymbol{a}\cdot\boldsymbol{b}=a_ib_i$), or a single contraction of adjacent indices of two tensors (e.g. $\boldsymbol{c}\cdot\boldsymbol{d}=c_{ij}d_{jk}$); the symbol ':' denotes an inner product of two second-order tensors (e.g. $\boldsymbol{c}:\boldsymbol{d}=c_{ij}d_{ij}$), or a double contraction of adjacent indices of tensors of ranks two and higher (e.g. $\boldsymbol{C}:\boldsymbol{\epsilon}^{\mathrm{e}}=C_{ijkl}\epsilon^{\mathrm{e}}_{kl}$); the symbol '$\otimes$' denotes a juxtaposition of two vectors, $(\boldsymbol{a}\otimes\boldsymbol{b})_{ij}=a_ib_j$, or of two symmetric second-order tensors, $(\boldsymbol{\alpha}\otimes\boldsymbol{\beta})_{ijkl}=\alpha_{ij}\beta_{kl}$.

2 Stability and ellipticity conditions for incrementally linear solids

We first define what we mean by ''material instability'' in the context of this paper. We use the nonlinear finite element flow chart of Fig. 1 as our backdrop since we intend to use this paper for boundary-value problem calculations. The flow chart identifies two types of bifurcation: global and local. Global bifurcation occurs at the structure level and includes as examples the Euler buckling of beams and snap-through and snap buckling of shells, among others. In the context of nonlinear finite element analysis, global bifurcation can be predicted from some 'test functions' of the overall global tangent stiffness matrix which change sign as the singular point is passed, such as the determinant, the minimum pivot, or the minimum eigenvalue of this matrix [17]. Local bifurcation, on the other hand, is analyzed at the Gauss integration points and entails the prediction of non-unique strain rate fields. Both types of bifurcation are checked at the conclusion of the global iteration loop when all types of iteration have converged. We equate ''material instability'' to local bifurcation and predict its occurrence at the Gauss point level.

2.1 Local bifurcation and uniqueness of solution

Consider a solid body defined by domain $\mathcal{B}$ and bounded by surface $\partial\mathcal{B}$, where the latter admits the decomposition $\partial\mathcal{B}=\overline{\partial\mathcal{B}_t\cup\partial\mathcal{B}_u}$ and $\emptyset=\partial\mathcal{B}_t\cap\partial\mathcal{B}_u$; and where $\partial\mathcal{B}_t$ and $\partial\mathcal{B}_u$ are portions of the entire boundary where traction rates and velocities are prescribed.

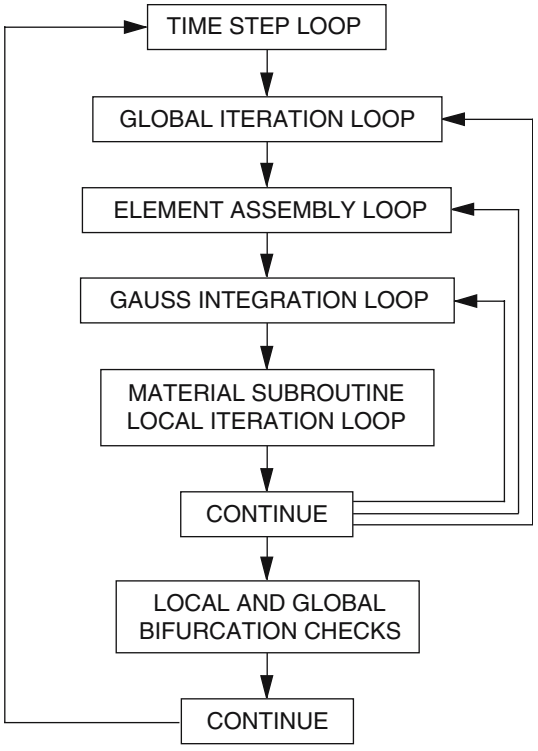

Fig. 1 Flow chart of nonlinear finite element algorithm with local and global bifurcation checks

Without loss of generality we consider a quasi-static problem and assume two possible local solutions arising for the first time within this domain. The solutions are denoted by the local Cauchy stress rate and velocity fields, $(\dot{\boldsymbol{\sigma}}, \dot{\boldsymbol{\sigma}}^*)$ and $(\boldsymbol{v}, \boldsymbol{v}^*)$, respectively. For the solution $(\dot{\boldsymbol{\sigma}}, \boldsymbol{v})$ to be admissible we must have

$$\begin{aligned} \operatorname{div}\dot{\boldsymbol{\sigma}} + \dot{\boldsymbol{f}} &= \boldsymbol{0} \quad \text{in } \mathcal{B}, \\ \boldsymbol{v} &= \dot{\boldsymbol{u}}_0 \quad \text{on } \partial\mathcal{B}_u, \\ \dot{\boldsymbol{\sigma}} \cdot \boldsymbol{n} &= \dot{\boldsymbol{t}}_0 \quad \text{on } \partial\mathcal{B}_t, \end{aligned} \tag{1}$$

where $\boldsymbol{f}$ is the body force vector per unit volume in the undeformed configuration, $\boldsymbol{n}$ is the unit outward normal to $\partial\mathcal{B}$, $\boldsymbol{u}_0$ and $\boldsymbol{t}_0$ are prescribed boundary displacements and nominal tractions, respectively, and div is the spatial divergence operator. For the alternative solution $(\dot{\boldsymbol{\sigma}}^*, \boldsymbol{v}^*)$ to be admissible it must also satisfy (1).

Next, we consider the integral

$$\int_{\mathcal{B}} \operatorname{div}[(\boldsymbol{v}^* - \boldsymbol{v}) \cdot (\dot{\boldsymbol{\sigma}}^* - \dot{\boldsymbol{\sigma}})] \mathrm{d}V = \int_{\mathcal{B}} (\dot{\boldsymbol{\epsilon}}^* - \dot{\boldsymbol{\epsilon}}) : (\dot{\boldsymbol{\sigma}}^* - \dot{\boldsymbol{\sigma}}) \mathrm{d}V + \int_{\mathcal{B}} (\boldsymbol{v}^* - \boldsymbol{v}) \cdot \operatorname{div}(\dot{\boldsymbol{\sigma}}^* - \dot{\boldsymbol{\sigma}}) \mathrm{d}V. \tag{2}$$

The second integral on the right-hand side vanishes since $\dot{\boldsymbol{\sigma}}$ and $\dot{\boldsymbol{\sigma}}^*$ both satisfy the partial differential equation in $\mathcal{B}$. The left-hand side can be transformed into a surface integral by Gauss theorem to yield

$$\int_{\mathcal{B}} \operatorname{div}[(\boldsymbol{v}^* - \boldsymbol{v}) \cdot (\dot{\boldsymbol{\sigma}}^* - \dot{\boldsymbol{\sigma}})] \mathrm{d}V = \int_{\partial\mathcal{B}} (\boldsymbol{v}^* - \boldsymbol{v}) \cdot (\dot{\boldsymbol{\sigma}}^* - \dot{\boldsymbol{\sigma}}) \cdot \boldsymbol{n} \mathrm{d}V = 0. \tag{3}$$

Thus, any pair of possible solutions must satisfy the condition

$$\int_{\mathcal{B}} (\dot{\boldsymbol{\epsilon}}^* - \dot{\boldsymbol{\epsilon}}) : (\dot{\boldsymbol{\sigma}}^* - \dot{\boldsymbol{\sigma}}) \mathrm{d}V = 0. \tag{4}$$

Uniqueness is guaranteed for every point and for every pair of stresses and strains linked by the constitutive equation if

$$(\dot{\boldsymbol{\epsilon}}^* - \dot{\boldsymbol{\epsilon}}) : (\dot{\boldsymbol{\sigma}}^* - \dot{\boldsymbol{\sigma}}) > 0 \tag{5}$$

pointwise in $\mathcal{B}$. The density expression on the left-hand side of (5) has been explored in detail by Hill [20], among others, and in the context of 'controllable incremental responses' by Nova [31] and Chambon [14].

2.2 Local stability for incrementally linear material

Consider the following incremental constitutive equation

$$\dot{\boldsymbol{\sigma}} = \boldsymbol{c} : \dot{\boldsymbol{\epsilon}}, \quad \dot{\boldsymbol{\sigma}}^* = \boldsymbol{c} : \dot{\boldsymbol{\epsilon}}^*, \quad \boldsymbol{c} = \frac{\partial \boldsymbol{\sigma}}{\partial \boldsymbol{\epsilon}} = \frac{\partial \boldsymbol{\sigma}^*}{\partial \boldsymbol{\epsilon}^*}, \tag{6}$$

where $\boldsymbol{c}$ is a tensor of constitutive moduli. Note that the same tensor $\boldsymbol{c}$ is used irrespective of the direction of the strain rate tensor. If $\boldsymbol{c}$ is invariant with respect to the direction of $\dot{\boldsymbol{\epsilon}}$, then we say that the material response is *incrementally linear*.

Definition of stability. An incrementally linear material is (incrementally) stable if

$$\boldsymbol{\phi} : \boldsymbol{c} : \boldsymbol{\phi} > 0 \tag{7}$$

for any symmetric second-order tensor $\boldsymbol{\phi} \neq \boldsymbol{0}$. Equation (7) is the *stability condition*. Note that this definition has no connection with stability theory in the sense of Lyapunov, see e.g., [30].

Now consider the kinematical jumps,

$$[\![\boldsymbol{v}]\!] = \boldsymbol{v}^* - \boldsymbol{v}, \quad [\![\dot{\boldsymbol{\epsilon}}]\!] = \dot{\boldsymbol{\epsilon}}^* - \dot{\boldsymbol{\epsilon}} = \mathrm{grad}^{\mathrm{s}}[\![\boldsymbol{v}]\!], \tag{8}$$

where $\mathrm{grad}^{\mathrm{s}}$ is the symmetric gradient operator. For an incrementally linear material violation of Eq. (7) for $\boldsymbol{\phi} \equiv [\![\dot{\boldsymbol{\epsilon}}]\!] \neq \boldsymbol{0}$ implies any of the conditions

$$[\![\dot{\boldsymbol{\epsilon}}]\!] : [\![\dot{\boldsymbol{\sigma}}]\!] = 0 : \quad \text{loss of stability/uniqueness;} \tag{9}$$

$$[\![\dot{\boldsymbol{\sigma}}]\!] = \boldsymbol{0} : \quad \text{continuity of stress rate tensor,} \tag{10}$$

where $[\![\dot{\boldsymbol{\sigma}}]\!] = \dot{\boldsymbol{\sigma}}^* - \dot{\boldsymbol{\sigma}} = \boldsymbol{c} : [\![\dot{\boldsymbol{\epsilon}}]\!]$ is the jump in the Cauchy stress rate field. Note that continuity of the stress rate for a non-zero $[\![\dot{\boldsymbol{\epsilon}}]\!]$ implies loss of stability/uniqueness, but the converse is not necessarily true. For example, if the constitutive tensor $\boldsymbol{c}$ does not possess the major symmetry, then the equations described above do not occur at the same time.

To elaborate the last paragraph, we write

$$[\![\dot{\boldsymbol{\epsilon}}]\!] : [\![\dot{\boldsymbol{\sigma}}]\!] = [\![\dot{\boldsymbol{\epsilon}}]\!] : \boldsymbol{c} : [\![\dot{\boldsymbol{\epsilon}}]\!] = [\![\dot{\boldsymbol{\epsilon}}]\!] : \mathrm{sym}(\boldsymbol{c}) : [\![\dot{\boldsymbol{\epsilon}}]\!] = 0, \tag{11}$$

where 'sym' denotes a major symmetry operator, i.e. $\mathrm{sym}(c_{ijkl}) = (c_{ijkl} + c_{klij})/2$. Hence, loss of stability/uniqueness is given by the condition

$$\det(\mathrm{sym}(\boldsymbol{c})) = 0, \tag{12}$$

where it is understood that the tensor $\boldsymbol{c}$ can be arranged into a 6×6 square matrix (for 3D problems) to obtain the determinant. On the other hand, continuity of the stress rate is equivalent to the homogeneous equation

$$[\![\dot{\boldsymbol{\sigma}}]\!] = \boldsymbol{c} : [\![\dot{\boldsymbol{\epsilon}}]\!] = \boldsymbol{0}, \tag{13}$$

and so for a non-trivial solution to exist we must have

$$\det(\boldsymbol{c}) = 0. \tag{14}$$

The eigenmode (or e-mode) of the singular symmetrized tensor $\mathrm{sym}(\boldsymbol{c})$ may be calculated from the homogeneous equation

$$\mathrm{sym}(\boldsymbol{c}) : [\![\dot{\boldsymbol{\epsilon}}]\!] = \boldsymbol{0}. \tag{15}$$

However, the above equation does not preclude a jump in the stress rate for a non-symmetric $\boldsymbol{c}$ since $\mathrm{sym}(\boldsymbol{c}) = \boldsymbol{c} - \mathrm{skw}(\boldsymbol{c})$, and so the jump in the stress rate is given by

$$[\![\dot{\boldsymbol{\sigma}}]\!] = \boldsymbol{c} : [\![\dot{\boldsymbol{\epsilon}}]\!] = \mathrm{skw}(\boldsymbol{c}) : [\![\dot{\boldsymbol{\epsilon}}]\!] \neq \boldsymbol{0}. \tag{16}$$

On the other hand, a more physically meaningful e-mode is the one obtained from the singular full tensor $\boldsymbol{c}$ via (13), which is consistent with a zero jump in the stress rate. Note that e-modes only describe deformation shapes but have no unique norms.

2.3 Strong ellipticity for incrementally linear material

Consider the following specific form for $[\![\dot{\boldsymbol{\epsilon}}]\!]$:

$$[\![\dot{\boldsymbol{\epsilon}}]\!] = \varphi \mathrm{sym}(\boldsymbol{m} \otimes \boldsymbol{n}), \tag{17}$$

where $\boldsymbol{m}$ and $\boldsymbol{n}$ are unit vectors, and φ is a scalar, real coefficient. In this case the determinant rank of the tensor $[\![\dot{\boldsymbol{\epsilon}}]\!]$ is one. Thus we get

$$[\![\dot{\boldsymbol{\epsilon}}]\!] : [\![\dot{\boldsymbol{\sigma}}]\!] = \varphi^2 \mathrm{sym}(\boldsymbol{m} \otimes \boldsymbol{n}) : \boldsymbol{c} : \mathrm{sym}(\boldsymbol{m} \otimes \boldsymbol{n}) = \varphi^2 \boldsymbol{m} \cdot \boldsymbol{A} \cdot \boldsymbol{m}, \tag{18}$$

where $\boldsymbol{A} = \boldsymbol{A}(\boldsymbol{n})$ is called the acoustic tensor, so named because of its connection to the propagation of planar waves [18]. This tensor has components

$$A_{ij} = n_k c_{ikjl} n_l. \tag{19}$$

Definition of strong ellipticity. An incrementally linear material is strongly elliptic if for any unit vectors $\boldsymbol{m}$ and $\boldsymbol{n}$,

$$\boldsymbol{m} \cdot \boldsymbol{A}(\boldsymbol{n}) \cdot \boldsymbol{m} > 0. \tag{20}$$

Equation (20) is the strong ellipticity condition. Since (17) is only a specific case of a more general tensor $[\![\dot{\boldsymbol{\epsilon}}]\!]$, it follows that a stable material is strongly elliptic.

Definition of ellipticity. An incrementally linear material is elliptic if for any unit vector $\boldsymbol{n}$,

$$\det(\boldsymbol{A}) \neq 0. \tag{21}$$

Note that ellipticity permits the scalar product $\boldsymbol{m} \cdot \boldsymbol{A} \cdot \boldsymbol{m}$ to be negative.

For the specific form of the jump tensor $[\![\dot{\boldsymbol{\epsilon}}]\!]$ given by (17) the following conditions are of interest

$$\boldsymbol{m} \cdot \boldsymbol{A} \cdot \boldsymbol{m} = 0 : \quad \text{loss of strong ellipticity;} \tag{22}$$

$$\boldsymbol{A} \cdot \boldsymbol{m} = \boldsymbol{0} : \quad \text{loss of ellipticity.} \tag{23}$$

Since $\boldsymbol{m} \cdot \boldsymbol{A} \cdot \boldsymbol{m} = \boldsymbol{m} \cdot \mathrm{sym}(\boldsymbol{A}) \cdot \boldsymbol{m}$, loss of strong ellipticity occurs when

$$\inf|_n \det(\mathrm{sym}(\boldsymbol{A})) = 0. \tag{24}$$

We use the "infimum" symbol here for the set of determinants since we are typically concerned with a condition that is initially strongly elliptic and we wish to find the critical state at which (24) is satisfied for the

first time. This requires that we search for the critical normal vector $\boldsymbol{n}$ that minimizes the determinant function for a given $\boldsymbol{c}$, though the latter tensor could also change with deformation. On the other hand, for a nontrivial solution to (23) to exist we must have

$$\inf|_n \det(\boldsymbol{A}) = 0. \tag{25}$$

Loss of ellipticity condition can be written in the alternative form

$$\boldsymbol{A}\cdot\boldsymbol{m} = [\boldsymbol{c} : \mathrm{sym}(\boldsymbol{m}\otimes\boldsymbol{n})]\cdot\boldsymbol{n} = \frac{1}{\varphi}[\![\dot{\boldsymbol{\sigma}}]\!]\cdot\boldsymbol{n} = \boldsymbol{0}. \tag{26}$$

We recognize $[\![\dot{\boldsymbol{\sigma}}]\!]\cdot\boldsymbol{n} = [\![\dot{\boldsymbol{t}}]\!]$ as the jump in the nominal traction rate vector across a line whose unit normal is $\boldsymbol{n}$. Such line is often associated with the boundary of a so-called ''deformation band.'' Thus, loss of ellipticity is equivalent to having a zero jump of the traction rate vector across the band. The eigenvector $\boldsymbol{m}$ of the singular tensor $\boldsymbol{A}$ along with the critical vector $\boldsymbol{n}$ at which this tensor becomes singular for the first time define the corresponding rank-one e-mode, $\mathrm{sym}(\boldsymbol{m}\otimes\boldsymbol{n})$, often called the ''slip tensor'' in the literature.

3 Elastoplasticity and comparison solids

For elastoplastic solids the constitutive tensor $\boldsymbol{c}$ depends on the loading direction $\dot{\boldsymbol{\epsilon}}$ and has two branches, one for elastic unloading and another for plastic loading, i.e.,

$$\boldsymbol{c} = \begin{cases} \boldsymbol{c}^{\mathrm{e}} & \text{for elastic unloading;} \\ \boldsymbol{c}^{\mathrm{ep}} & \text{for plastic loading,} \end{cases} \tag{27}$$

where $\boldsymbol{c}^{\mathrm{e}}$ and $\boldsymbol{c}^{\mathrm{ep}}$ are the elastic and elastoplastic tangent constitutive operators, respectively. The latter has the following prototype structure for classical plasticity

$$\boldsymbol{c}^{\mathrm{ep}} = \boldsymbol{c}^{\mathrm{e}} - \boldsymbol{c}^{\mathrm{p}},\quad \boldsymbol{c}^{\mathrm{p}} = \frac{1}{\chi}\boldsymbol{c}^{\mathrm{e}} : \boldsymbol{g}\otimes\boldsymbol{f} : \boldsymbol{c}^{\mathrm{e}},\quad \chi = \boldsymbol{f} : \boldsymbol{c}^{\mathrm{e}} : \boldsymbol{g} + H > 0, \tag{28}$$

where $\boldsymbol{f}$ and $\boldsymbol{g}$ are symmetric stress gradient tensors to the yield and plastic potential surfaces, respectively, and H is the generalized plastic modulus. For associative flow rule, $\boldsymbol{g} = \boldsymbol{f}$. Hardening is defined by the condition $H > 0$, softening by the condition $H < 0$, and perfect plasticity by the condition $H = 0$. Loading and unloading depends on the direction of the so-called trial rate of stress, $\boldsymbol{c}^{\mathrm{e}} : \dot{\boldsymbol{\epsilon}}$, relative to the yield function, and is determined from the criterion

$$\mathrm{sgn}(\boldsymbol{f} : \boldsymbol{c}^{\mathrm{e}} : \dot{\boldsymbol{\epsilon}}) = \begin{cases} (-) & \text{for elastic unloading;} \\ (+) & \text{for plastic loading.} \end{cases} \tag{29}$$

Throughout we assume that $\boldsymbol{c}^{\mathrm{e}}$ is positive definite and possesses the major and minor symmetry.

3.1 Comparison solid for associative plasticity

Because $\boldsymbol{c}$ has two branches the response is incrementally nonlinear in the sense that the constitutive tangent operator depends on the direction of the strain rate. This requires that we consider all possible loading/unloading scenarios and choose the most critical one. Herein we take associative plasticity, $\boldsymbol{g} = \boldsymbol{f}$, and assume $\boldsymbol{f} : \boldsymbol{c}^{\mathrm{e}} : \dot{\boldsymbol{\epsilon}} > 0$ and $\boldsymbol{f} : \boldsymbol{c}^{\mathrm{e}} : \dot{\boldsymbol{\epsilon}}^{*} > 0$. Thus, both solutions follow the plastic loading branch. This ''comparison solid'' was introduced by Hill [19] to establish a bound or limit to the stable region for associative plasticity.

The consistency condition for the solution $\dot{\boldsymbol{\epsilon}}$ is given by

$$\boldsymbol{f} : \boldsymbol{c}^{\mathrm{e}} : (\dot{\boldsymbol{\epsilon}} - \dot{\lambda}\boldsymbol{f}) - \dot{\lambda}H = 0, \tag{30}$$

where $\dot{\lambda} \geq 0$ is the plastic consistency multiplier. Solving for $\dot{\lambda}$, we obtain

$$\dot{\lambda} = \frac{1}{\chi}\boldsymbol{f} : \boldsymbol{c}^{\mathrm{e}} : \dot{\boldsymbol{\epsilon}},\quad \chi = \boldsymbol{f} : \boldsymbol{c}^{\mathrm{e}} : \boldsymbol{f} + H > 0. \tag{31}$$

The last inequality limits the degree of softening. Similarly, for the solution $\dot{\boldsymbol{\epsilon}}^{*}$ the consistency condition is written as

$$\boldsymbol{f} : \boldsymbol{c}^{\mathrm{e}} : (\dot{\boldsymbol{\epsilon}} + [\![\dot{\boldsymbol{\epsilon}}]\!] - \dot{\bar{\lambda}}\boldsymbol{f}) - \dot{\bar{\lambda}}H = 0, \tag{32}$$

from which the new consistency parameter may be determined as

$$\dot{\bar{\lambda}} = \dot{\lambda} + \dot{\tilde{\lambda}} \geq 0,\quad \dot{\tilde{\lambda}} = \frac{1}{\chi}\boldsymbol{f} : \boldsymbol{c}^{\mathrm{e}} : [\![\dot{\boldsymbol{\epsilon}}]\!] \geq 0. \tag{33}$$

It is important to note that $\dot{\boldsymbol{\epsilon}}$ and $[\![\dot{\boldsymbol{\epsilon}}]\!]$ are two independent kinematical variables, so $\dot{\bar{\lambda}} \geq 0$ is guaranteed only if both $\dot{\lambda} \geq 0$ and $\dot{\tilde{\lambda}} \geq 0$. The inequality for $\dot{\tilde{\lambda}}$ guarantees that in the loading/loading combination the solution corresponding to $\dot{\boldsymbol{\epsilon}}^{*}$ continues to yield plastically past and beyond the solution corresponding to $\dot{\boldsymbol{\epsilon}}$, thus permitting a clear characterization of the modes of failure at bifurcation.

For Hill's comparison solid the power density produced by the jumps is given by

$$\mathcal{L}_1 = [\![\dot{\boldsymbol{\epsilon}}]\!] : [\![\dot{\boldsymbol{\sigma}}]\!] = [\![\dot{\boldsymbol{\epsilon}}]\!] : \boldsymbol{c}^{\mathrm{ep}} : [\![\dot{\boldsymbol{\epsilon}}]\!] = [\![\dot{\boldsymbol{\epsilon}}]\!] : (\boldsymbol{c}^{\mathrm{e}} - \boldsymbol{c}^{\mathrm{p}}) : [\![\dot{\boldsymbol{\epsilon}}]\!] > 0. \tag{34}$$

The symbol "$\mathcal{L}$" connotes either a stable region "limiter" or a "lower bound" to all possible powers as elaborated below. For continuous loading $\mathcal{L}_1$ is expected to cross the zero value first before any jumps-induced power density derived from other possible loading/unloading combinations. To elaborate the last point, assume that $\boldsymbol{f} : \boldsymbol{c}^{\mathrm{e}} : \dot{\boldsymbol{\epsilon}} > 0$ (plastic loading) and $\boldsymbol{f} : \boldsymbol{c}^{\mathrm{e}} : \dot{\boldsymbol{\epsilon}}^* < 0$ (elastic unloading). Then $\dot{\boldsymbol{\sigma}} = \boldsymbol{c}^{\mathrm{ep}} : \dot{\boldsymbol{\epsilon}}$ and $\dot{\boldsymbol{\sigma}}^* = \boldsymbol{c}^{\mathrm{e}} : \dot{\boldsymbol{\epsilon}}^*$. The jump in the stress rate in this case is

$$[\![\dot{\boldsymbol{\sigma}}]\!] = \boldsymbol{c}^{\mathrm{e}} : \dot{\boldsymbol{\epsilon}}^* - \boldsymbol{c}^{\mathrm{ep}} : \dot{\boldsymbol{\epsilon}} = \boldsymbol{c}^{\mathrm{e}} : [\![\dot{\boldsymbol{\epsilon}}]\!] + \boldsymbol{c}^{\mathrm{p}} : \dot{\boldsymbol{\epsilon}}. \tag{35}$$

The corresponding power density is given by

$$\mathcal{P} = [\![\dot{\boldsymbol{\epsilon}}]\!] : [\![\dot{\boldsymbol{\sigma}}]\!] = [\![\dot{\boldsymbol{\epsilon}}]\!] : \boldsymbol{c}^{\mathrm{e}} : [\![\dot{\boldsymbol{\epsilon}}]\!] + [\![\dot{\boldsymbol{\epsilon}}]\!] : \boldsymbol{c}^{\mathrm{p}} : \dot{\boldsymbol{\epsilon}}. \tag{36}$$

Subtracting (34) from (36) and using the definition of $\boldsymbol{c}^{\mathrm{p}}$ from (28) gives

$$\begin{aligned} \mathcal{P} - \mathcal{L}_1 &= [\![\dot{\boldsymbol{\epsilon}}]\!] : \boldsymbol{c}^{\mathrm{p}} : [\![\dot{\boldsymbol{\epsilon}}]\!] + [\![\dot{\boldsymbol{\epsilon}}]\!] : \boldsymbol{c}^{\mathrm{p}} : \dot{\boldsymbol{\epsilon}} \\ &= \frac{1}{\chi} \underbrace{([\![\dot{\boldsymbol{\epsilon}}]\!] : \boldsymbol{c}^{\mathrm{e}} : \boldsymbol{f})}_{<0} \underbrace{(\boldsymbol{f} : \boldsymbol{c}^{\mathrm{e}} : \dot{\boldsymbol{\epsilon}}^*)}_{<0} > 0. \end{aligned} \tag{37}$$

Thus $\mathcal{L}_1 < \mathcal{P}$, and so $\mathcal{L}_1$ serves as a "lower bound" to $\mathcal{P}$. A similar result may be obtained if instead we assume that $\boldsymbol{f} : \boldsymbol{c}^{\mathrm{e}} : \dot{\boldsymbol{\epsilon}} < 0$ and $\boldsymbol{f} : \boldsymbol{c}^{\mathrm{e}} : \dot{\boldsymbol{\epsilon}}^* > 0$ (unloading/loading combination); or if we assume that $\boldsymbol{f} : \boldsymbol{c}^{\mathrm{e}} : \dot{\boldsymbol{\epsilon}} < 0$ and $\boldsymbol{f} : \boldsymbol{c}^{\mathrm{e}} : \dot{\boldsymbol{\epsilon}}^* < 0$ (unloading/unloading combination). By ensuring that $\mathcal{L}_1 > 0$, we exclude any local bifurcation.

3.2 Comparison solid for non-associative plasticity

If the flow rule is non-associative the condition $\boldsymbol{f} : \boldsymbol{c}^{\mathrm{e}} : \dot{\boldsymbol{\epsilon}} > 0$ no longer implies that $\boldsymbol{g} : \boldsymbol{c}^{\mathrm{e}} : \dot{\boldsymbol{\epsilon}} > 0$, so we cannot proceed with a similar analysis as in Sect. 3.1. For this case Raniecki and Bruhns [36] proposed a comparison solid producing a power density of the form

$$\mathcal{L}_2 = [\![\dot{\boldsymbol{\epsilon}}]\!] : [\![\dot{\boldsymbol{\sigma}}]\!] = [\![\dot{\boldsymbol{\epsilon}}]\!] : \tilde{\boldsymbol{c}}^{\mathrm{ep}} : [\![\dot{\boldsymbol{\epsilon}}]\!] = [\![\dot{\boldsymbol{\epsilon}}]\!] : (\boldsymbol{c}^{\mathrm{e}} - \tilde{\boldsymbol{c}}^{\mathrm{p}}) : [\![\dot{\boldsymbol{\epsilon}}]\!] > 0, \tag{38}$$

where

$$\tilde{\boldsymbol{c}}^{\mathrm{p}} = \frac{1}{4r\chi} \boldsymbol{c}^{\mathrm{e}} : (\boldsymbol{g} + r\boldsymbol{f}) \otimes (\boldsymbol{g} + r\boldsymbol{f}) : \boldsymbol{c}^{\mathrm{e}} \quad \forall r > 0. \tag{39}$$

This comparison solid is purely fictitious in the sense that there is no real material described by such a constitutive tangent operator, but the expression for $\mathcal{L}_2$ does serve as a lower bound to all possible power densities in the non-associative regime. For example, consider first the case $\boldsymbol{f} : \boldsymbol{c}^{\mathrm{e}} : \dot{\boldsymbol{\epsilon}} > 0$ and $\boldsymbol{f} : \boldsymbol{c}^{\mathrm{e}} : \dot{\boldsymbol{\epsilon}}^* > 0$ (plastic loading for both solutions). Following (33) we augment the restriction $\boldsymbol{f} : \boldsymbol{c}^{\mathrm{e}} : [\![\dot{\boldsymbol{\epsilon}}]\!] \geq 0$. The jump in the Cauchy stress rate is then $[\![\dot{\boldsymbol{\sigma}}]\!] = \boldsymbol{c}^{\mathrm{ep}} : [\![\dot{\boldsymbol{\epsilon}}]\!]$, yielding a power density of the form

$$\mathcal{U} = [\![\dot{\boldsymbol{\epsilon}}]\!] : \boldsymbol{c}^{\mathrm{ep}} : [\![\dot{\boldsymbol{\epsilon}}]\!] = [\![\dot{\boldsymbol{\epsilon}}]\!] : \left(\boldsymbol{c}^{\mathrm{e}} - \frac{1}{\chi} \boldsymbol{c}^{\mathrm{e}} : \boldsymbol{g} \otimes \boldsymbol{f} : \boldsymbol{c}^{\mathrm{e}} \right) : [\![\dot{\boldsymbol{\epsilon}}]\!]. \tag{40}$$

Subtracting (38) from (40) gives

$$4r\chi(\mathcal{U} - \mathcal{L}_2) = \{[\![\dot{\boldsymbol{\epsilon}}]\!] : \boldsymbol{c}^{\mathrm{e}} : (\boldsymbol{g} - r\boldsymbol{f})\}^2 \geq 0. \tag{41}$$

Since $4r\chi > 0$ then $\mathcal{U} \geq \mathcal{L}_2$, and so $\mathcal{L}_2$ is a lower bound to $\mathcal{P}$. Note that $\mathcal{U} = \mathcal{L}_2$ when $\boldsymbol{g} = \boldsymbol{f}$ and $r = 1$.

We need to consider other possible loading and unloading combinations, so we next assume that $b_1 \equiv \boldsymbol{f} : \boldsymbol{c}^{\mathrm{e}} : \dot{\boldsymbol{\epsilon}} > 0$ and $b_2 \equiv \boldsymbol{f} : \boldsymbol{c}^{\mathrm{e}} : \dot{\boldsymbol{\epsilon}}^* < 0$ (loading/unloading combination); then $\dot{\boldsymbol{\sigma}} = \boldsymbol{c}^{\mathrm{ep}} : \dot{\boldsymbol{\epsilon}}$ and $\dot{\boldsymbol{\sigma}}^* = \boldsymbol{c}^{\mathrm{e}} : \dot{\boldsymbol{\epsilon}}^*$. The jump in the stress rate is then given by $[\![\dot{\boldsymbol{\sigma}}]\!] = \boldsymbol{c}^{\mathrm{e}} : [\![\dot{\boldsymbol{\epsilon}}]\!] + \boldsymbol{c}^{\mathrm{p}} : \dot{\boldsymbol{\epsilon}}$, and the corresponding power density is

$$\mathcal{P} = [\![\dot{\boldsymbol{\epsilon}}]\!] : \boldsymbol{c}^{\mathrm{e}} : [\![\dot{\boldsymbol{\epsilon}}]\!] + \frac{1}{\chi} [\![\dot{\boldsymbol{\epsilon}}]\!] : \boldsymbol{c}^{\mathrm{e}} : \boldsymbol{g} \otimes \boldsymbol{f} : \boldsymbol{c}^{\mathrm{e}} : \dot{\boldsymbol{\epsilon}}. \tag{42}$$

Setting $a = [\![\dot{\boldsymbol{\epsilon}}]\!] : \boldsymbol{c}^{\mathrm{e}} : \boldsymbol{g}$ and subtracting $\mathcal{L}_2$ from (42) yields

$$\begin{aligned} 4r\chi(\mathcal{P} - \mathcal{L}_2) &= 4rab_1 + [a + r(b_2 - b_1)]^2 \\ &= \underbrace{[a + r(b_1 + b_2)]^2}_{>0} \underbrace{-4r^2 b_1 b_2}_{>0} > 0, \end{aligned} \tag{43}$$

so $\mathcal{L}_2$ is also a lower bound to $\mathcal{P}$. For the unloading/loading combination a similar result may be obtained by simply reversing the signs of b_1 and b_2. Finally, for the unloading/unloading combination the condition is less critical, so we have again exhausted all possible combinations and conclude that by keeping $\mathcal{L}_2 > 0$ we exclude all possible local bifurcations.

An "in-loading comparison solid" is one for which $\mathcal{U}$ represents the power density induced by the jumps. It is not possible to show that $\mathcal{U}$ is a lower bound to $\mathcal{P}$ as given by (42), for example, unless the flow rule is associative, since $\boldsymbol{g}$ could deviate significantly from $\boldsymbol{f}$ depending on the degree of non-associativity. Hence, no inequality relation exists between $\mathcal{U}$ and $\mathcal{P}$. On the other hand, $\mathcal{U} = 0$ does result in loss of stability by

definition (7), so $\mathcal{U}$ is sometimes called an ''upper bound.''

A question arises as to what value of $r > 0$ provides for the ''optimal'' estimate of the size of the stability region. By ''optimal'' we mean the value of r at which we can get as far into the loading history as possible before the exclusion condition $\mathcal{L}_2 > 0$ is violated for the first time. To answer this question it suffices to note that $\mathcal{L}_2 > 0$ implies

$$\boldsymbol{\phi} : \tilde{\boldsymbol{c}}^{\mathrm{ep}} : \boldsymbol{\phi} = \boldsymbol{\phi} : \boldsymbol{c}^{\mathrm{e}} : \boldsymbol{\phi} - \frac{1}{4r\chi}[(\boldsymbol{\phi} : \boldsymbol{c}^{\mathrm{e}} : (\boldsymbol{g} + r\boldsymbol{f})]^2 > 0 \quad \forall r > 0 \tag{44}$$

for all symmetric second-order tensor $\boldsymbol{\phi} \neq \boldsymbol{0}$. By the Cauchy–Schwarz inequality we have (see [3] for proof)

$$[(\boldsymbol{\phi} : \boldsymbol{c}^{\mathrm{e}} : (\boldsymbol{g} + r\boldsymbol{f})]^2 \leq (\boldsymbol{\phi} : \boldsymbol{c}^{\mathrm{e}} : \boldsymbol{\phi})[(\boldsymbol{g} + r\boldsymbol{f}) : \boldsymbol{c}^{\mathrm{e}} : (\boldsymbol{g} + r\boldsymbol{f})]. \tag{45}$$

Thus, (44) is satisfied provided we satisfy the stronger condition

$$\boldsymbol{\phi} : \boldsymbol{c}^{\mathrm{e}} : \boldsymbol{\phi}\left[1 - \frac{1}{4r\chi}(\boldsymbol{g} + r\boldsymbol{f}) : \boldsymbol{c}^{\mathrm{e}} : (\boldsymbol{g} + r\boldsymbol{f})\right] \geq 0. \tag{46}$$

Now, since $\boldsymbol{c}^{\mathrm{e}}$ is positive definite, we must have

$$\chi \geq \frac{1}{4r}(\boldsymbol{g} + r\boldsymbol{f}) : \boldsymbol{c}^{\mathrm{e}} : (\boldsymbol{g} + r\boldsymbol{f}), \tag{47}$$

from which the optimal value of r is obtained as

$$r_{\mathrm{opt}} = \left(\frac{\boldsymbol{g} : \boldsymbol{c}^{\mathrm{e}} : \boldsymbol{g}}{\boldsymbol{f} : \boldsymbol{c}^{\mathrm{e}} : \boldsymbol{f}}\right)^{1/2}. \tag{48}$$

The optimal constitutive tensor $\tilde{\boldsymbol{c}}^{\mathrm{ep}}_{\mathrm{opt}}$ for the comparison solid is then obtained by substituting r_{opt} in (39).

3.3 Deformation banding

For non-associative plasticity an exclusion condition against loss of strong ellipticity is given by

$$\boldsymbol{m} \cdot \boldsymbol{A} \cdot \boldsymbol{m} > 0,$$
$$\boldsymbol{A} = \boldsymbol{n} \cdot \left[\boldsymbol{c}^{\mathrm{e}} - \frac{1}{4r\chi}\boldsymbol{c}^{\mathrm{e}} : (\boldsymbol{g} + r\boldsymbol{f}) \otimes (\boldsymbol{g} + r\boldsymbol{f}) : \boldsymbol{c}^{\mathrm{e}}\right] \cdot \boldsymbol{n}, \tag{49}$$

for all $\boldsymbol{m}, \boldsymbol{n} \neq \boldsymbol{0}$ and $r > 0$. The acoustic tensor in this case is symmetric even if $\boldsymbol{g} \neq \boldsymbol{f}$. A condition that guarantees loss of strong ellipticity for the real material is given by

$$\boldsymbol{m} \cdot \mathrm{sym}(\boldsymbol{A}) \cdot \boldsymbol{m} = 0, \quad \boldsymbol{A} = \boldsymbol{n} \cdot \left[\boldsymbol{c}^{\mathrm{e}} - \frac{1}{\chi}\boldsymbol{c}^{\mathrm{e}} : \boldsymbol{g} \otimes \boldsymbol{f} : \boldsymbol{c}^{\mathrm{e}}\right] \cdot \boldsymbol{n}. \tag{50}$$

In this case the constitutive operator pertains to the ''in-loading'' comparison solid. For a non-symmetric $\boldsymbol{A}$ this criterion satisfies the continuum boundary value problem (1) but does not preclude a traction rate jump across a potential band. In fact this jump is given by

$$\begin{aligned}[\![\dot{\boldsymbol{t}}]\!] &= \boldsymbol{n} \cdot [\![\dot{\boldsymbol{\sigma}}]\!] = \varphi \boldsymbol{A} \cdot \boldsymbol{m} \\ &= \varphi[\mathrm{sym}(\boldsymbol{A}) + \mathrm{skw}(\boldsymbol{A})] \cdot \boldsymbol{m} = \varphi\, \mathrm{skw}(\boldsymbol{A}) \cdot \boldsymbol{m} \neq \boldsymbol{0},\end{aligned} \tag{51}$$

since we must have $\mathrm{sym}(\boldsymbol{A}) \cdot \boldsymbol{m} = \boldsymbol{0}$ if $\mathrm{sym}(\boldsymbol{A})$ is singular. On the other hand, even if the jump is not zero, $\boldsymbol{m} \cdot [\![\dot{\boldsymbol{t}}]\!] = 0$ due to the orthogonality generated by a skew-symmetric operator. Bigoni and Zaccaria [5] showed that (49) and (50) are coincident under the hypothesis of isotropy.

A more physically meaningful solution is obtained by enforcing the condition of zero traction rate jump across a potential deformation band, leading to the homogeneous equation

$$\boldsymbol{A} \cdot \boldsymbol{m} = \boldsymbol{0}, \quad \boldsymbol{A} = \boldsymbol{n} \cdot \left[\boldsymbol{c}^{\mathrm{e}} - \frac{1}{\chi}\boldsymbol{c}^{\mathrm{e}} : \boldsymbol{g} \otimes \boldsymbol{f} : \boldsymbol{c}^{\mathrm{e}}\right] \cdot \boldsymbol{n}. \tag{52}$$

In this case we want to find a unit vector $\boldsymbol{n}$ where $\det(\boldsymbol{A}) = 0$ is satisfied for the first time. Equation (52) is the localization condition presented by Rudnicki and Rice [40], without the geometric terms. In the following we shall assume that all eigenvalues of $\boldsymbol{A}$ are real to exclude a so-called flutter instability, which could occur with complex eigenvalues [38].

Rice and Rudnicki [39] demonstrated that for a deformation band-mode, bifurcation of the ''in-loading'' comparison solid occurs first before any other possible loading/unloading modes. For the sake of completeness we outline a slightly different (and more concise) proof of their result below. Let

$$\boldsymbol{A}^{\mathrm{e}} = \boldsymbol{n} \cdot \boldsymbol{c}^{\mathrm{e}} \cdot \boldsymbol{n}, \quad \boldsymbol{\alpha} = \boldsymbol{n} \cdot \boldsymbol{c}^{\mathrm{e}} : \boldsymbol{g}, \quad \boldsymbol{\beta} = \boldsymbol{f} : \boldsymbol{c}^{\mathrm{e}} \cdot \boldsymbol{n}. \tag{53}$$

Then the acoustic tensor can be written as

$$\boldsymbol{A} = \boldsymbol{A}^{\mathrm{e}} - \frac{1}{\chi}\boldsymbol{\alpha} \otimes \boldsymbol{\beta}. \tag{54}$$

Let χ_{LL} denote the specific value of the plastic divisor χ for the ''in-loading'' comparison solid at which $\boldsymbol{A}$ is singular, i.e.,

$$\left(\boldsymbol{A}^{\mathrm{e}} - \frac{1}{\chi_{\mathrm{LL}}}\boldsymbol{\alpha}\otimes\boldsymbol{\beta}\right)\cdot\boldsymbol{m} = \boldsymbol{0}, \tag{55}$$

where subscript ''LL'' denotes a loading/loading mode. For non-trivial solutions to exist the vector $\boldsymbol{A}^{\mathrm{e}}\cdot\boldsymbol{m}$ must be parallel to $\boldsymbol{\alpha}$, and

$$\chi_{\mathrm{LL}} = \boldsymbol{\alpha}\cdot\boldsymbol{A}^{\mathrm{e}-1}\cdot\boldsymbol{\beta}, \tag{56}$$

assuming the elastic part of the acoustic tensor is invertible (which is normally the case).

Now, consider an unloading/loading combination and assume that $\boldsymbol{f}:\boldsymbol{c}^{\mathrm{e}}:\dot{\boldsymbol{\epsilon}} < 0$ and $\boldsymbol{f}:\boldsymbol{c}^{\mathrm{e}}:\dot{\boldsymbol{\epsilon}}^{*} > 0$, where $\dot{\boldsymbol{\epsilon}}^{*} = \dot{\boldsymbol{\epsilon}} + [\![\dot{\boldsymbol{\epsilon}}]\!] = \dot{\boldsymbol{\epsilon}} + \varphi\mathrm{sym}(\boldsymbol{m}\otimes\boldsymbol{n})$. We can think of $\dot{\boldsymbol{\epsilon}}$ and $\dot{\boldsymbol{\epsilon}}^{*}$ as the strain rates ''outside'' and ''inside'' the band, respectively, although the terms ''outside'' and ''inside'' are interchangeable in this context. The jump in the stress rate is given by (35) in this case, and setting $\boldsymbol{n}\cdot[\![\dot{\boldsymbol{\sigma}}]\!] = \boldsymbol{0}$ gives

$$\varphi\left(\boldsymbol{A}^{\mathrm{e}} - \frac{1}{\chi_{\mathrm{UL}}}\boldsymbol{\alpha}\otimes\boldsymbol{\beta}\right)\cdot\boldsymbol{m} = \frac{1}{\chi_{\mathrm{UL}}}(\boldsymbol{f}:\boldsymbol{c}^{\mathrm{e}}:\dot{\boldsymbol{\epsilon}})\boldsymbol{\alpha}, \tag{57}$$

where subscript ''UL'' indicates an unloading/loading mode. The acoustic tensor above is non-singular since $\chi_{\mathrm{UL}} \neq \chi_{\mathrm{LL}}$, and in fact its inverse has a closed-form expression given by the Sherman–Morrison formula as

$$\boldsymbol{A}^{-1}_{\mathrm{UL}} := \left(\boldsymbol{A}^{\mathrm{e}} - \frac{1}{\chi_{\mathrm{UL}}}\boldsymbol{\alpha}\otimes\boldsymbol{\beta}\right)^{-1} = \boldsymbol{A}^{\mathrm{e}-1} + \frac{\boldsymbol{A}^{\mathrm{e}-1}\cdot\boldsymbol{\alpha}\otimes\boldsymbol{\beta}\cdot\boldsymbol{A}^{\mathrm{e}-1}}{\chi_{\mathrm{UL}} - \chi_{\mathrm{LL}}}. \tag{58}$$

Thus, (57) gives

$$\varphi\boldsymbol{m} = \left(\frac{\boldsymbol{f}:\boldsymbol{c}^{\mathrm{e}}:\dot{\boldsymbol{\epsilon}}}{\chi_{\mathrm{UL}} - \chi_{\mathrm{LL}}}\right)\boldsymbol{A}^{\mathrm{e}-1}\cdot\boldsymbol{\alpha}. \tag{59}$$

The inequality for loading ''inside the band'' can be expanded as

$$\boldsymbol{f}:\boldsymbol{c}^{\mathrm{e}}:[\dot{\boldsymbol{\epsilon}} + \mathrm{sym}(\varphi\boldsymbol{m}\otimes\boldsymbol{n})] = \boldsymbol{f}:\boldsymbol{c}^{\mathrm{e}}:\dot{\boldsymbol{\epsilon}}\left(1 + \frac{\chi_{\mathrm{LL}}}{\chi_{\mathrm{UL}} - \chi_{\mathrm{LL}}}\right) > 0, \tag{60}$$

upon substitution of $\varphi\boldsymbol{m}$ from (59). Since $\boldsymbol{f}:\boldsymbol{c}^{\mathrm{e}}:\dot{\boldsymbol{\epsilon}} < 0$ by hypothesis, it follows that

$$\frac{\chi_{\mathrm{UL}}}{\chi_{\mathrm{UL}} - \chi_{\mathrm{LL}}} < 0. \tag{61}$$

The plastic divisors χ_{LL} and χ_{UL} are always positive to ensure nonnegative plastic consistency parameters; hence, we must have the inequality $\chi_{\mathrm{UL}} < \chi_{\mathrm{LL}}$. This implies that deformation banding with unloading on one side and loading on the other side is possible only when the plastic modulus H_{UL} is less than the critical modulus H_{LL}. Now, if H is assumed to degrade in a smooth fashion from the stable region up to the moment of localization, then it follows that the loading/loading mode is more critical since it requires a higher value of H to localize. Borre and Maier [13, p 39], demonstrated that the singularity of the acoustic tensor $\boldsymbol{A}$ is a sufficient condition for bifurcation.

4 Isotropy, singularities and e-modes

Numerous elastoplastic constitutive models in geomechanics have been developed based on the assumption of isotropy. Isotropic models are useful for capturing mechanical responses under monotonic loading. Furthermore, isotropic functions have some nice mathematical features that render a physically meaningful solution. This section exploits these features in the mathematical capture of the triggering of some interesting bifurcation modes in collapsible solids.

4.1 Spectral representation

We begin with an isotropic linearly elastic material where the stress and elastic strain tensors $\boldsymbol{\sigma}$ and $\boldsymbol{\epsilon}^{\mathrm{e}}$ are coaxial with the eigenvectors $\{\boldsymbol{n}^{(1)},\boldsymbol{n}^{(2)},\boldsymbol{n}^{(3)}\}$ defining their principal directions. These tensors admit the spectral representation

$$\boldsymbol{\sigma} = \sum_{A=1}^{3}\sigma_A\boldsymbol{n}^{(A)}\otimes\boldsymbol{n}^{(A)}, \quad \boldsymbol{\epsilon}^{\mathrm{e}} = \sum_{A=1}^{3}\epsilon^{\mathrm{e}}_A\boldsymbol{n}^{(A)}\otimes\boldsymbol{n}^{(A)}, \tag{62}$$

where the scalar coefficients are the correspondng principal values. The Cauchy stress rate can be written in spectral form as [32]

$$\dot{\boldsymbol{\sigma}} = \sum_{A=1}^{3}\dot{\sigma}_A\boldsymbol{n}^{(A)}\otimes\boldsymbol{n}^{(A)} + \sum_{A=1}^{3}\sum_{B\neq A}\omega_{AB}(\sigma_B - \sigma_A)\boldsymbol{n}^{(A)}\otimes\boldsymbol{n}^{(B)}, \tag{63}$$

and the elastic strain rate as

$$\dot{\boldsymbol{\epsilon}}^{\mathrm{e}} = \sum_{A=1}^{3}\dot{\epsilon}^{\mathrm{e}}_A\boldsymbol{n}^{(A)}\otimes\boldsymbol{n}^{(A)} + \sum_{A=1}^{3}\sum_{B\neq A}\omega_{AB}(\epsilon^{\mathrm{e}}_B - \epsilon^{\mathrm{e}}_A)\boldsymbol{n}^{(A)}\otimes\boldsymbol{n}^{(B)}, \tag{64}$$

where ω_{AB} is the AB-component of the skew-symmetric spin tensor $\boldsymbol{\omega}$, which is the same for the two tensors to preserve coaxiality.

The stress gradient tensors $\boldsymbol{f}$ and $\boldsymbol{g}$ also admit the spectral representations

$$\boldsymbol{f} = \sum_{A=1}^{3} f_A \boldsymbol{n}^{(A)} \otimes \boldsymbol{n}^{(A)}, \quad \boldsymbol{g} = \sum_{A=1}^{3} g_A \boldsymbol{n}^{(A)} \otimes \boldsymbol{n}^{(A)}, \tag{65}$$

where the coefficients are the corresponding gradients with respect to the principal stresses. Now, by the additive decomposition of the total strain rate into elastic and plastic parts, and by the flow rule, we get

$$\begin{aligned} \dot{\boldsymbol{\epsilon}} &= \dot{\boldsymbol{\epsilon}}^{\mathrm{e}} + \dot{\boldsymbol{\epsilon}}^{\mathrm{p}} = \dot{\boldsymbol{\epsilon}}^{\mathrm{e}} + \dot{\lambda}\boldsymbol{g} \\ &= \sum_{A=1}^{3} \underbrace{(\dot{\epsilon}_A^{\mathrm{e}} + \dot{\lambda} g_A)}_{\dot{\epsilon}_A} \boldsymbol{n}^{(A)} \otimes \boldsymbol{n}^{(A)} \\ &\quad + \sum_{A=1}^{3} \sum_{B \neq A} \omega_{AB} (\epsilon_B^{\mathrm{e}} - \epsilon_A^{\mathrm{e}}) \boldsymbol{n}^{(A)} \otimes \boldsymbol{n}^{(B)}, \end{aligned} \tag{66}$$

where $\dot{\epsilon}_A$ represents the total principal strain rate and $\dot{\lambda} \geq 0$ is the plastic consistency parameter. The above equation indicates that the spin of the total strain is the same as the spin of the elastic strain, a sensible result in light of the absence of plastic spin in infinitesimal plasticity theory.

Accordingly, the elastoplastic constitutive operator $\boldsymbol{c}^{\mathrm{ep}}$ admits the spectral representation

$$\begin{aligned} \boldsymbol{c}^{\mathrm{ep}} &= \boldsymbol{c}^{\mathrm{e}} - \frac{1}{\chi} \boldsymbol{c}^{\mathrm{e}} : \boldsymbol{g} \otimes \boldsymbol{f} : \boldsymbol{c}^{\mathrm{e}} \\ &= \sum_{A=1}^{3} \sum_{B=1}^{3} a_{AB}^{\mathrm{ep}} \boldsymbol{m}^{(A)} \otimes \boldsymbol{m}^{(B)} \\ &\quad + \frac{1}{2} \sum_{A=1}^{3} \sum_{B \neq A} \left(\frac{\sigma_B - \sigma_A}{\epsilon_B^{\mathrm{e}} - \epsilon_A^{\mathrm{e}}} \right) (\boldsymbol{m}^{(AB)} \otimes \boldsymbol{m}^{(AB)} \\ &\quad + \boldsymbol{m}^{(AB)} \otimes \boldsymbol{m}^{(BA)}), \end{aligned} \tag{67}$$

where

$$\begin{aligned} a_{AB}^{\mathrm{ep}} &:= \frac{\partial \sigma_A}{\partial \epsilon_B} = a_{AB}^{\mathrm{e}} - \frac{1}{\chi} \left(\sum_{C=1}^{3} f_C a_{CA}^{\mathrm{e}} \right) \left(\sum_{D=1}^{3} a_{BD}^{\mathrm{e}} g_D \right), \\ \chi &= \boldsymbol{f} : \boldsymbol{c}^{\mathrm{e}} : \boldsymbol{g} + H = \sum_{A=1}^{3} \sum_{B=1}^{3} f_A a_{AB}^{\mathrm{e}} g_B + H. \end{aligned} \tag{68}$$

The notations are as follows: $\boldsymbol{m}^{(A)} = \boldsymbol{n}^{(A)} \otimes \boldsymbol{n}^{(A)}$, $\boldsymbol{m}^{(AB)} = \boldsymbol{n}^{(A)} \otimes \boldsymbol{n}^{(B)}$, $[a_{AB}^{\mathrm{e}}] = [\partial \sigma_A / \partial \epsilon_B^{\mathrm{e}}]$ is the matrix of elastic moduli in principal axes (this is a 3×3 matrix for 3D problems), and $[a_{AB}^{\mathrm{ep}}] = [\partial \sigma_A / \partial \epsilon_B]$ is the corresponding matrix of elastoplastic tangential moduli in principal axes.

4.2 Singularity of $\boldsymbol{c}^{\mathrm{ep}}$ and associated e-modes

Consider an alternative solution $\dot{\boldsymbol{\sigma}}^*$, also given in spectral form as

$$\dot{\boldsymbol{\sigma}}^* = \sum_{A=1}^{3} \dot{\sigma}_A^* \boldsymbol{n}^{(A)} \otimes \boldsymbol{n}^{(A)} + \sum_{A=1}^{3} \sum_{B \neq A} \omega_{AB}^* (\sigma_B - \sigma_A) \boldsymbol{n}^{(A)} \otimes \boldsymbol{n}^{(B)}. \tag{69}$$

Our description of this alternative stress rate tensor remains reckoned with respect to the existing stress state characterized by the same principal values and principal directions as those used for the stress rate $\dot{\boldsymbol{\sigma}}$ in (63). Now, subtracting (69) from (63) gives the jump in the stress rate

$$\begin{aligned} [\![\dot{\boldsymbol{\sigma}}]\!] &= \sum_{A=1}^{3} [\![\dot{\sigma}_A]\!] \boldsymbol{n}^{(A)} \otimes \boldsymbol{n}^{(A)} \\ &\quad + \sum_{A=1}^{3} \sum_{B \neq A} [\![\omega_{AB}]\!] (\sigma_B - \sigma_A) \boldsymbol{n}^{(A)} \otimes \boldsymbol{n}^{(B)}, \end{aligned} \tag{70}$$

where $[\![\dot{\sigma}_A]\!] = \dot{\sigma}_A^* - \dot{\sigma}_A$ and $[\![\omega_{AB}]\!] = \omega_{AB}^* - \omega_{AB}$. The jump in the stress rate tensor (six elements for 3D problems) consists of jumps in the principal values of the stress rates (three elements) and jumps in the spins (three elements).

The conjugate total strain rate that drives the alternative stress rate $\dot{\boldsymbol{\sigma}}^*$ also admits the spectral representation

$$\dot{\boldsymbol{\epsilon}}^* = \sum_{A=1}^{3} \dot{\epsilon}_A^* \boldsymbol{n}^{(A)} \otimes \boldsymbol{n}^{(A)} + \sum_{A=1}^{3} \sum_{B \neq A} \omega_{AB}^* (\epsilon_B^{\mathrm{e}} - \epsilon_A^{\mathrm{e}}) \boldsymbol{n}^{(A)} \otimes \boldsymbol{n}^{(B)}. \tag{71}$$

Once again, to preserve coaxiality the spins of the tensors $\dot{\boldsymbol{\sigma}}^*$ and $\dot{\boldsymbol{\epsilon}}^*$ must be the same. Accordingly, the jump in the total strain rate is

$$\begin{aligned} [\![\dot{\boldsymbol{\epsilon}}]\!] &= \sum_{A=1}^{3} [\![\dot{\epsilon}_A]\!] \boldsymbol{n}^{(A)} \otimes \boldsymbol{n}^{(A)} \\ &\quad + \sum_{A=1}^{3} \sum_{B \neq A} [\![\omega_{AB}]\!] (\epsilon_B^{\mathrm{e}} - \epsilon_A^{\mathrm{e}}) \boldsymbol{n}^{(A)} \otimes \boldsymbol{n}^{(B)}. \end{aligned} \tag{72}$$

Now we consider the ''in-loading'' comparison solid described in Sec. 3.2 and write the jump in the stress rate at the moment of loss of uniqueness, see Eq. (10), as

$$[\![\dot{\boldsymbol{\sigma}}]\!] = \boldsymbol{c}^{\mathrm{ep}} : [\![\dot{\boldsymbol{\epsilon}}]\!] = \boldsymbol{0}, \tag{73}$$

where $\boldsymbol{c}^{\mathrm{ep}}$ admits the spectral decomposition (67). In order for the jump in stress rate to vanish the jumps in

the principal values and the jumps in the spins must be zero, i.e.,

$$[\![\dot{\sigma}_A]\!] = 0, \quad A = 1,2,3, \qquad [\![\omega_{AB}]\!] = 0 \quad \forall A \neq B. \tag{74}$$

For non-trivial solution we must have $\det(\boldsymbol{c}^{\mathrm{ep}}) = 0$. The singularities of $\boldsymbol{c}^{\mathrm{ep}}$, however, are of two types, characterized by the following equations, see [32]

$$\text{(a)} \quad \det(a^{\mathrm{ep}}_{AB}) = 0, \tag{75}$$

$$\text{(b)} \quad \sigma_A = \sigma_B, \quad A \neq B. \tag{76}$$

Type (a) corresponds to a singularity of the 3×3 elastoplastic matrix in principal axes, whereas type (b) singularity gives rise to indeterminate spins. Each type of singularity generates a specific e-mode.

To obtain the corresponding e-modes we first consider type (a) singularity. The homogeneous problem

$$[\![\dot{\sigma}_A]\!] = \sum_{B=1}^{3} a^{\mathrm{ep}}_{AB}[\![\dot{\epsilon}_B]\!] = 0 \tag{77}$$

results in non-trivial values for $[\![\dot{\epsilon}_B]\!]$ if and only if the coefficient matrix is singular. Now, from (70) if $\sigma_A \neq \sigma_B$ for $A \neq B$ the only way that $[\![\dot{\boldsymbol{\sigma}}]\!]$ can vanish is for the spins to vanish, i.e., $[\![\omega_{AB}]\!] = 0$. Thus type (a) singularity gives rise to an e-mode of the form

$$[\![\dot{\boldsymbol{\epsilon}}]\!] = \sum_{A=1}^{3} [\![\dot{\epsilon}_A]\!] \boldsymbol{n}^{(A)} \otimes \boldsymbol{n}^{(A)}, \tag{78}$$

where $\{[\![\dot{\epsilon}_A]\!]\}$ is the e-mode of the singular matrix $[a^{\mathrm{ep}}_{AB}]$. In this case, bifurcation is characterized by jumps in the principal strain rates *at fixed principal axes*.

Next we consider type (b) singularity. Since the matrix $[a^{\mathrm{ep}}_{AB}]$ is non-singular then (77) only admits the trivial solution $[\![\dot{\epsilon}_A]\!] = 0$ for $A = 1,2,3$. The corresponding e-mode is then

$$[\![\dot{\boldsymbol{\epsilon}}]\!] = [\![\omega_{AB}]\!](\epsilon^{\mathrm{e}}_B - \epsilon^{\mathrm{e}}_A)\boldsymbol{n}^{(A)} \otimes \boldsymbol{n}^{(B)} \tag{79}$$

for any $A \neq B$ where $\sigma_A = \sigma_B$. This is a ''pure shearing'' e-mode *at fixed principal values* and produces only rotation of principal axes. If the singularities of $\boldsymbol{c}^{\mathrm{ep}}$ are of both types (a) and (b) then the jump in the strain rate is given by the full tensor (72). Regardless of the type of singularity the e-mode has no unique norm.

4.3 Singularity of $\boldsymbol{A}$ and associated e-modes

Singularity of the acoustic tensor $\boldsymbol{A}$ does not follow from the singularity of $\boldsymbol{c}^{\mathrm{ep}}$; in fact if $\boldsymbol{A}$ is singular then $\boldsymbol{c}^{\mathrm{ep}}$ cannot be singular (unless the e-modes are constrained) since the singularity of the former leads to a rank-one e-mode whereas the singularity of the latter leads to a full-rank jump tensor $[\![\dot{\boldsymbol{\epsilon}}]\!]$ as shown in the previous section. The e-mode corresponding to a singular $\boldsymbol{A}$ is the rank-one tensor sym $(\boldsymbol{m} \otimes \boldsymbol{n})$, where $\boldsymbol{n}$ is the unit vector that identifies the zero minimum determinant of $\boldsymbol{A}$, and

$$\boldsymbol{m} = \pm \frac{\boldsymbol{A}^{\mathrm{e}-1} \cdot \boldsymbol{\alpha}}{\left\| \boldsymbol{A}^{\mathrm{e}-1} \cdot \boldsymbol{\alpha} \right\|} \tag{80}$$

is the eigenvector of $\boldsymbol{A}$. The correct sign for $\boldsymbol{m}$ is chosen by imposing condition (33),

$$\boldsymbol{f} : \boldsymbol{c}^{\mathrm{e}} : \mathrm{sym}(\boldsymbol{m} \otimes \boldsymbol{n}) \geq 0 \tag{81}$$

which guarantees that in the loading/loading solution the material ''inside'' the band continues to yield plastically past and beyond the material ''outside'' the band. Thus the tensor sym$(\boldsymbol{m} \otimes \boldsymbol{n})$ is well defined.

The trace of sym$(\boldsymbol{m} \otimes \boldsymbol{n})$, equal to the vector dot product $\boldsymbol{m} \cdot \boldsymbol{n}$, determines the nature of deformation band created at localization. Borja and Aydin [10] describe a classification scheme for deformation band types according to the following framework:

$$\begin{cases} \boldsymbol{m} \cdot \boldsymbol{n} = 1: & \text{pure dilation band;} \\ 0 < \boldsymbol{m} \cdot \boldsymbol{n} < 1: & \text{dilatant shear band;} \\ \boldsymbol{m} \cdot \boldsymbol{n} = 0: & \text{simple shear band;} \\ -1 < \boldsymbol{m} \cdot \boldsymbol{n} < 0: & \text{compactive shear band;} \\ \boldsymbol{m} \cdot \boldsymbol{n} = -1: & \text{pure compaction band.} \end{cases} \tag{82}$$

In a simple shear band the instantaneous relative movement is tangent to the band. In a dilatant (compactive) shear band the angle between the unit vectors $\boldsymbol{n}$ and $\boldsymbol{m}$ is acute (obtuse), and thus the band exhibits some form of instantaneous expansion (contraction). Pure dilation and pure compaction bands exhibit little or no shear offset. Because condition (81) requires that the tensor sym$(\boldsymbol{m} \otimes \boldsymbol{n})$ be oriented approximately in the direction of the stress gradient tensor $\boldsymbol{f}$, we can expect a compactive (dilative) bifurcation mode to occur on the compression (tension) cap of the yield surface.

4.4 Volume implosion and compaction banding

Volume implosion (explosion) and compaction (dilation) banding both result in pore collapse (growth) in

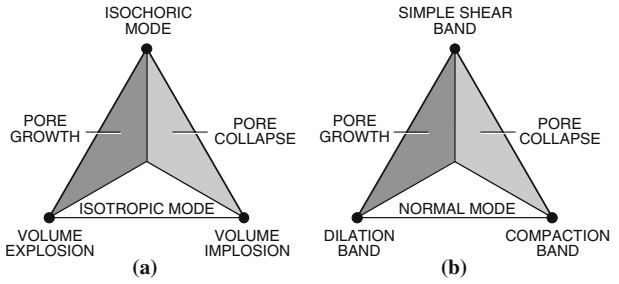

Fig. 2 Idealized diagrams defining failure modes in collapsible solids: (**a**) full-rank jump of strain rate tensor; (**b**) rank-one jump

soils and rocks. Volume implosion is diffuse whereas compaction banding is localized to a narrow tabular zone. In Fig. 2 we compare the kinematical signatures of these two types of bifurcation.

We first recall type (a) singularity of the constitutive tangent operator $\boldsymbol{c}^{\mathrm{ep}}$. The associated singular coefficient matrix $[a^{\mathrm{ep}}_{AB}]$ leads to jumps in the principal values of the strain rate tensor at fixed principal directions. The e-mode $\{[\![\dot{\epsilon}_A]\!]\}$ generally characterizes ''squashing'' and ''stretching'' in the direction of the principal axes (see Fig. 3a), with the net overall volumetric strain rate jump given by

$$[\![\dot{\epsilon}_{\mathrm{v}}]\!] = \sum_{A=1}^{3} [\![\dot{\epsilon}_A]\!]. \tag{83}$$

If $[\![\dot{\epsilon}_{\mathrm{v}}]\!] = 0$, then the e-mode is isochoric.

Consider a singular 3×3 matrix of elastoplastic coefficients $[a_{AB}]$ of rank two (for brevity we drop the superscript ''ep''). Assume that the first 2×2 submatrix is invertible so that the first two components of the e-mode can be solved for in terms of the third component. An e-mode normalized with respect to $[\![\dot{\epsilon}_3]\!]$ can be written as

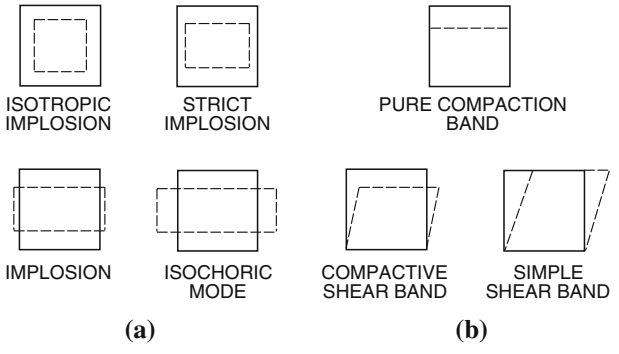

Fig. 3 E-modes leading to pore collapse for: (**a**) singular tangent constitutive operator; (**b**) singular tangent acoustic tensor

$$\{[\![\dot{\epsilon}_A]\!]\} = \frac{1}{a_{11}a_{22} - a_{12}a_{21}} \begin{Bmatrix} a_{12}a_{23} - a_{13}a_{22} \\ a_{13}a_{21} - a_{11}a_{23} \\ a_{11}a_{22} - a_{12}a_{21} \end{Bmatrix} = \frac{1}{\mathrm{cof}(a_{33})} \begin{Bmatrix} \mathrm{cof}(a_{31}) \\ \mathrm{cof}(a_{32}) \\ \mathrm{cof}(a_{33}) \end{Bmatrix}, \tag{84}$$

provided $\mathrm{cof}(a_{33}) \neq 0$, where cof = cofactor. Thus, the condition for an isochoric e-mode normalized with respect to $[\![\dot{\epsilon}_B]\!]$ is

$$\sum_{A=1}^{3} \mathrm{cof}(a_{BA}) = 0, \quad \mathrm{cof}(a_{BB}) \neq 0. \tag{85}$$

Consider the same singular 3×3 matrix $[a_{AB}]$. Its e-mode normalized with respect to $[\![\dot{\epsilon}_B]\!]$ is isotropic if

$$\mathrm{cof}(a_{B1}) = \mathrm{cof}(a_{B2}) = \mathrm{cof}(a_{B3}) \neq 0. \tag{86}$$

Isochoric and isotropic e-modes represent two ends of diffuse bifurcation arising from type (a) singularity of $\boldsymbol{c}^{\mathrm{ep}}$ (note that type (b) singularity of $\boldsymbol{c}^{\mathrm{ep}}$ leads to an isochoric e-mode). In general the actual bifurcation mode always lies between these two end modes.

Since an e-mode is a non-trivial solution of a system of homogeneous equations, its negative, $-[\![\dot{\epsilon}_A]\!]$, also satisfies the homogeneous equations. To choose the appropriate sign of the e-mode we again impose condition (33) for the ''in-loading'' comparison solid,

$$\boldsymbol{f} : \boldsymbol{c}^{\mathrm{e}} : [\![\dot{\boldsymbol{\epsilon}}]\!] = \sum_{A=1}^{3}\sum_{B=1}^{3} f_A a^{\mathrm{e}}_{AB} [\![\dot{\epsilon}_B]\!] > 0. \tag{87}$$

Thus, the volume jump is explosive (implosive) depending on whether the stress point at bifurcation is on the dilative (compactive) side of the yield surface.

Next we consider deformation banding-type of instability. Assuming isotropy the spectral form of the acoustic tensor may be written as

$$\begin{aligned} \boldsymbol{A} = &\sum_{A=1}^{3}\sum_{B=1}^{3} a^{\mathrm{ep}}_{AB} \cos\theta_A \cos\theta_B \boldsymbol{n}^{(A)} \otimes \boldsymbol{n}^{(B)} \\ &+ \frac{1}{2}\sum_{A=1}^{3}\sum_{B\neq A} \left(\frac{\sigma_B - \sigma_A}{\epsilon^{\mathrm{e}}_B - \epsilon^{\mathrm{e}}_A}\right)(\cos^2\theta_B \boldsymbol{n}^{(A)} \otimes \boldsymbol{n}^{(A)} \\ &+ \cos\theta_A \cos\theta_B \boldsymbol{n}^{(A)} \otimes \boldsymbol{n}^{(B)}), \end{aligned} \tag{88}$$

where $\cos\theta_A = \boldsymbol{n} \cdot \boldsymbol{n}^{(A)}$ (same for B). We are interested in finding a vector $\boldsymbol{n}$ at which $\inf(\det(\boldsymbol{A})) = 0$, as well as the associated eigenvector $\boldsymbol{m}$ of the singular

tensor. If $\boldsymbol{m} = \pm\boldsymbol{n}$ then we have a compaction/dilation band, and for this mode we set

$$\boldsymbol{A}\cdot\boldsymbol{n} = \sum_{A=1}^{3}\sum_{B=1}^{3} a_{AB}^{\mathrm{ep}} \cos\theta_A \cos^2\theta_B \boldsymbol{n}^{(A)} + \frac{1}{2}\sum_{A=1}^{3}\sum_{B\neq A}\left(\frac{\sigma_B-\sigma_A}{\epsilon_B^{\mathrm{e}}-\epsilon_A^{\mathrm{e}}}\right)\cos\theta_A\cos^2\theta_B\boldsymbol{n}^{(A)} = \boldsymbol{0}. \tag{89}$$

This vector equation can have a solution if and only if $\boldsymbol{n} = \boldsymbol{n}^{(A)}$, i.e., if $\boldsymbol{n}$ is parallel to any of the three principal axes. The spin terms drop out, and we are left with the condition for compaction/dilation banding, see [10],

$$a_{AA}^{\mathrm{ep}} = 0 \quad (\text{no sum on } A). \tag{90}$$

This means that a pure compaction/dilation band will emerge if $\boldsymbol{A}$ is singular at the same time that a diagonal element of $[a_{AB}^{\mathrm{ep}}]$ is zero. Like the framework for diffuse bifurcation, the localization condition for pure compaction/dilation banding does not entail rotation of the principal axes since the second summation terms in (89) drop out when we set $\boldsymbol{m} = \pm\boldsymbol{n}$. Figure 3b shows different modes of deformation banding characterized by pore collapse [10].

5 Simulation of pore collapse instabilities

Due to a large array of possible bifurcation modes, we shall limit the discussion of this section to two failure modes dominated by pore collapse instability, namely, volume implosion and compaction banding. Conditions for the occurrence of these two modes are summarized in Box 1.

Box 1 Conditions for volume implosion and compaction banding in collapsible solids (see Fig. 3)

Volume implosion:
1. Determinant condition: $\det(a_{AB}^{\mathrm{ep}}) = 0$
2. E-mode: $\sum_B a_{AB}^{\mathrm{ep}}[\![\dot{\epsilon}_B]\!] = 0$; $[\![\dot{\boldsymbol{\epsilon}}]\!] = \sum_A [\![\dot{\epsilon}_A]\!]\boldsymbol{m}^{(A)}$
3. Sign of e-mode: $\boldsymbol{f} : \boldsymbol{c}^{\mathrm{e}} : [\![\dot{\boldsymbol{\epsilon}}]\!] > 0$
4. Implosive when: $\mathrm{tr}([\![\dot{\boldsymbol{\epsilon}}]\!]) < 0$
5. Strictly implosive when: $[\![\dot{\epsilon}_A]\!] < 0$ for $A = 1, 2, 3$.

Compaction banding:
1. Determinant condition: $\inf|_n \det(\boldsymbol{A}) = 0$
2. E-mode: $\boldsymbol{A}\cdot\boldsymbol{m} = 0$; $[\![\dot{\boldsymbol{\epsilon}}]\!] = \varphi\,\mathrm{sym}(\boldsymbol{m}\otimes\boldsymbol{n})$
3. Sign of e-mode: $\boldsymbol{f} : \boldsymbol{c}^{\mathrm{e}} : \mathrm{sym}(\boldsymbol{m}\otimes\boldsymbol{n}) > 0$
4. Compactive shear band when: $\boldsymbol{m}\cdot\boldsymbol{n} < 0$
5. Pure compaction band when: $\boldsymbol{m} = -\boldsymbol{n}$

5.1 Associative plasticity

We consider a porous sandstone whose elastoplastic response is described by the three-invariant yield criterion [23, 25, 26]

$$F = (F_1 + c_3F_2)^{\mu}\bar{I}_1 + \kappa \le 0, \quad F_1 = \bar{I}_1^2/\bar{I}_2, \quad F_2 = \bar{I}_1^3/\bar{I}_3, \tag{91}$$

where c_3 and μ are material parameters (adopting the notations of [9]), and

$$\bar{I}_1 = \bar{\sigma}_1 + \bar{\sigma}_2 + \bar{\sigma}_3, \quad \bar{I}_2 = \bar{\sigma}_1\bar{\sigma}_2 + \bar{\sigma}_2\bar{\sigma}_3 + \bar{\sigma}_1\bar{\sigma}_3, \quad \bar{I}_3 = \bar{\sigma}_1\bar{\sigma}_2\bar{\sigma}_3 \tag{92}$$

are invariants defined from translated principal stresses

$$\bar{\sigma}_1 = \sigma_1 - a, \quad \bar{\sigma}_2 = \sigma_2 - a \quad \bar{\sigma}_3 = \sigma_3 - a. \tag{93}$$

The parameter $a > 0$ is a stress offset along the hydrostatic axis accommodating the material cohesion ($a = 0$ for cohesionless material). Typical values of $c_3 = 0.0013$ and $\mu = 0.5$ have been reported by Kim and Lade [23] for sandstone. Figure 4 shows a three-dimensional plot of the yield surface $F = 0$ in principal stress space for these values of c_3 and μ.

We assume that the plastic internal variable κ varies with plastic volumetric strain according to the expression

$$\kappa = a_1 v^{\mathrm{p}} \exp(a_2 v^{\mathrm{p}}), \quad v^{\mathrm{p}} = v_0^{\mathrm{p}} + \int_t \mathrm{tr}(\dot{\boldsymbol{\epsilon}}^{\mathrm{p}})\mathrm{d}t, \tag{94}$$

where a_1 and a_2 are material parameters that vary according to porosity of the rock (in principle, these parameters can be calibrated from the stress-strain mechanical responses exhibited by the rock). Highly porous rocks with a collapsible grain structure could exhibit pronounced softening response as they are

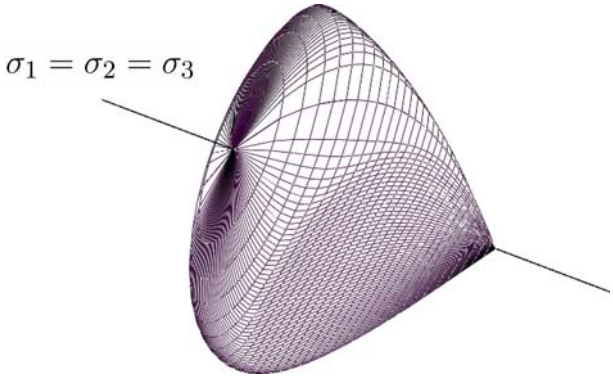

Fig. 4 Yield surface for sandstone

compressed, and this is reflected by the values of material parameters. In this study we shall take the values $a_1 = 200$ MPa and $a_2 = 100$ so that a softening response occurs when the plastic compaction reaches the value $v^p = -1\%$ [9]. In the simulations below we take Young's modulus $E = 100$ MPa, Poisson's ratio $\bar{\nu} = 0.20$, cohesion parameter $a = 10$ kPa, and reference plastic strain $v_0^p = -0.005$; initial stresses are assumed as $\sigma_{11} = \sigma_{22} = \sigma_{33} = -100$ kPa (isotropic). The plasticity model is integrated using the classical return mapping algorithm described by Borja et al. [12].

We consider the following strain-driven load path: $\Delta\epsilon_{11} = -0.005\%$; $\Delta\epsilon_{22} = +0.003\%$; $\Delta\epsilon_{33} = -0.001\%$; $\Delta\gamma_{12} = 2\Delta\epsilon_{12} = +0.002\%$; $\Delta\gamma_{23} = \Delta\gamma_{13} = 0$. This leads to an imposed net volumetric strain increment $\Delta\epsilon_v = -0.003\%$ (compressive) as well as to a rotation of principal axes on plane 1–2.

Figure 5 plots the determinant functions $\det(a^{ep}_{AB})$ and $\inf|_n \det(\boldsymbol{A})$. We recall from Sec. 3.1 that violation of the exclusion condition for the Hill comparison solid signifies initial bifurcation, which in this example is detected at load step number 168 (each load step consists of applying the above strain increments). The jumps in the principal strain rates normalized to have a unit norm are: $[\![\dot{\epsilon}_A]\!] = \{-0.845, -0.165, 0.516\}$, resulting in $\mathrm{tr}([\![\dot{\boldsymbol{\epsilon}}]\!]) < 0$. As expected, the predicted e-mode is implosive, although not ''strictly implosive'' according to the definition in Box 1 (not all principal jumps are compressive). On the other hand, a compactive shear band is predicted much later, at load step number 288. For the compactive shear band mode calculation of the critical orientations of $\boldsymbol{n}$ was done numerically by sweeping the 1–2 plane in one degree-increments. The minimum determinant of $\boldsymbol{A}$ vanishes on plane 1–2 at orientations $\boldsymbol{n}$ defined by $\theta_n = 29°$ and 137° relative to the positive 1-axis (conjugate modes). The calculated eigenvectors $\boldsymbol{m}$ are at orientations $\theta_m = 137°$ and 29°, respectively, also relative to the positive one-axis. In both conjugate deformation bands the angle between the vectors $\boldsymbol{n}$ and $\boldsymbol{m}$ is 108°, so $\boldsymbol{m} \cdot \boldsymbol{n} = -0.31 < 0$ affirming a compactive shear band.

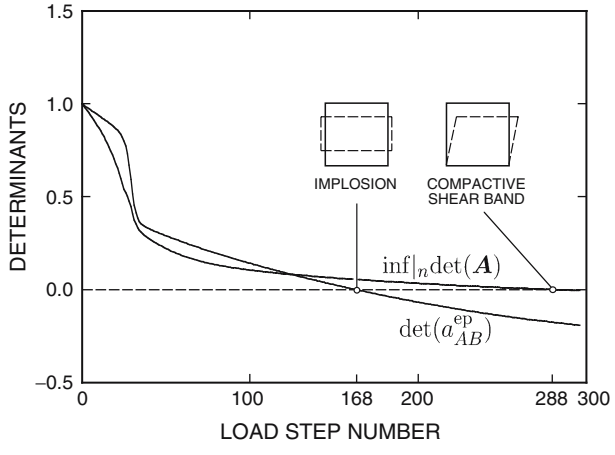

Fig. 5 Normalized determinants (with respect to initial values) of tangent constitutive matrix and tangent acoustic tensor, associative plasticity case

5.2 Non-associative plasticity

For the next simulations we consider a plastic potential function of the form

$$G = (-\bar{c}_0 + F_1 + c_3 F_3)^{\nu} \bar{I}_1 + \text{constant}. \tag{95}$$

Figure 6 shows 3D plots of this function in principal stress space for exponent value $\nu = 0.25$ and for different values of parameter $\bar{c}_0$ characteristic of plain concrete and other frictional materials [23]. The parameter $\bar{c}_0$ evidently controls the degree of volumetric non-associativity of the plastic flow. Figure 7 superimposes the plastic potential surface with $\bar{c}_0 = 3.0$ with the yield surface of Sect. 5.1 on a meridian plane defined by the hydrostatic axis and one of the three principal stress axes. It is seen that the flow rule is approximately associative only near the nose but rapidly exhibits a nearly deviatoric character away from the hydrostatic axis. This non-associative volumetric plastic flow response is consistent with observed plastic flow behavior of many frictional materials such as rock, concrete, and sand [23].

We now repeat the procedure outlined in Sect. 5.1 and plot the determinant functions in Fig. 8. The matrix $[a^{ep}_{AB}]$ for the ''in-loading'' comparison solid becomes singular at step number 174, where the accompanying e-mode exhibits an implosive character defined by principal values $[\![\dot{\epsilon}_A]\!] = \{-0.845, -0.163, +0.509\}$ again normalized to have a unit norm. This e-mode compares well with that calculated in Sect. 5.1. However, a pure compaction band is detected at a much earlier stage of the simulation, at step number 12, where the determinant of the acoustic tensor vanishes for the first time. This is corroborated by the elasto-plastic modulus component a^{ep}_{11} reversing in sign from positive to negative at the same step number 12 (this defines the direction of the normal to the compaction band, see [9]). The critical orientation of $\boldsymbol{n}$ is calculated at $\theta_n = 173°$, and there is no conjugate band. The associated orientation of $\boldsymbol{m}$ is calculated at $\theta_m = -7°$, so the angle between the two vectors is 180°, affirming a compaction band. Clearly, this example underscores the significant sensitivity of a deformation band-type instability prediction to degree of non-associativity of the plastic flow.

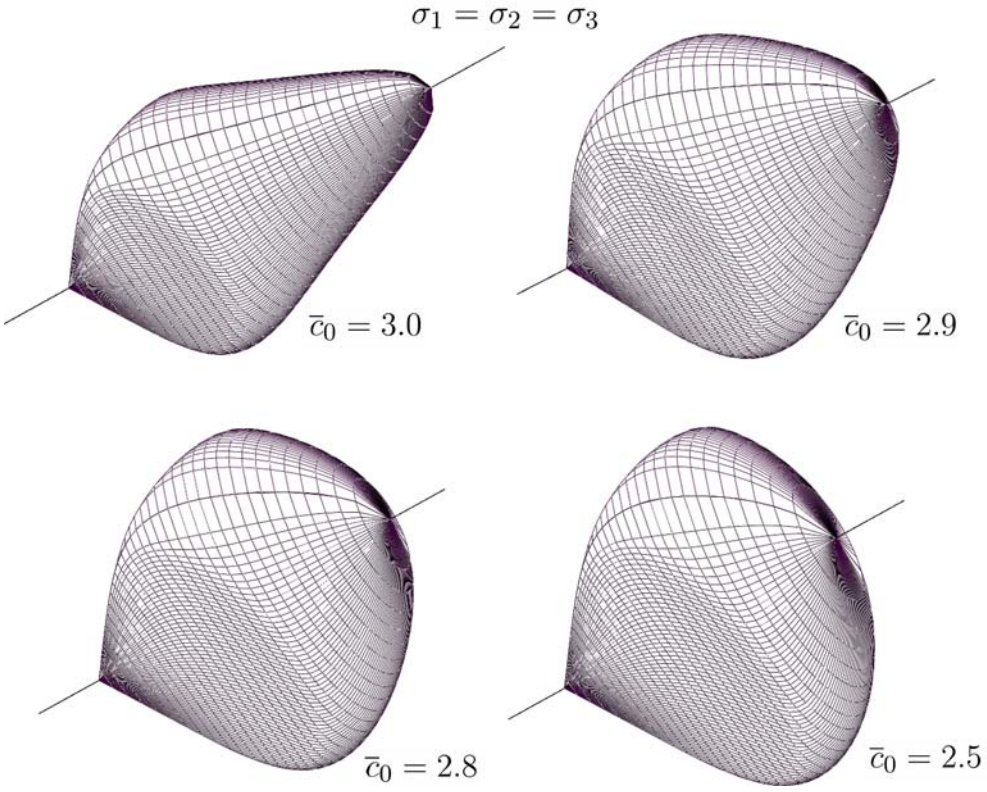

Fig. 6 Family of plastic potential surfaces for sandstone

For non-associative isotropic plasticity the optimal constitutive tensor for the comparison solid of Raniecki and Bruhns [36] also admits the spectral representation

$$\tilde{\boldsymbol{c}}^{\mathrm{ep}}_{\mathrm{opt}} = \sum_{A=1}^{3}\sum_{B=1}^{3} \tilde{a}^{\mathrm{ep}}_{AB}\boldsymbol{m}^{(A)} \otimes \boldsymbol{m}^{(B)} + \frac{1}{2}\sum_{A=1}^{3}\sum_{B\neq A}\left(\frac{\sigma_B - \sigma_A}{\epsilon^{\mathrm{e}}_B - \epsilon^{\mathrm{e}}_A}\right)(\boldsymbol{m}^{(AB)} \otimes \boldsymbol{m}^{(AB)} + \boldsymbol{m}^{(AB)} \otimes \boldsymbol{m}^{(BA)}), \tag{96}$$

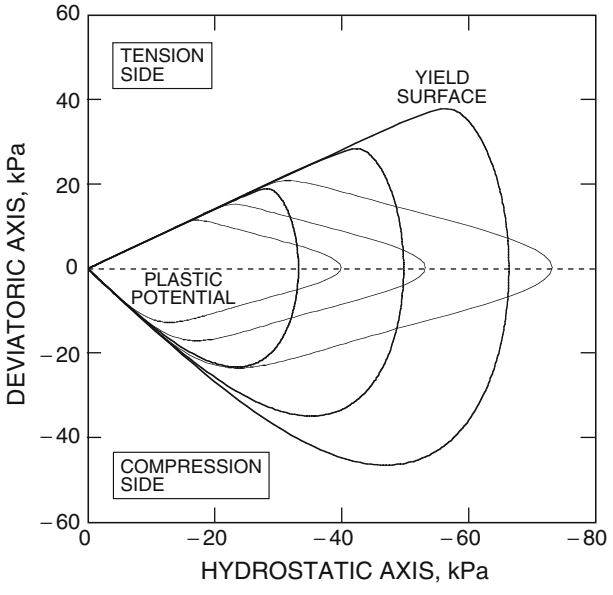

Fig. 7 Fan of yield and plastic potential surfaces for sandstone

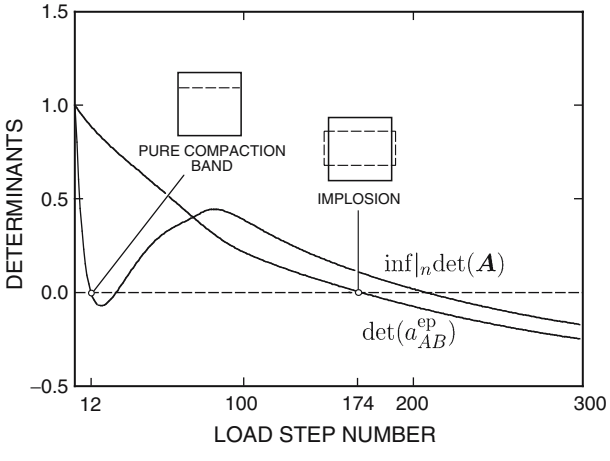

Fig. 8 Normalized determinants (with respect to initial values) of tangent constitutive matrix and tangent acoustic tensor, non-associative plasticity case

where

$$\tilde{a}^{\mathrm{ep}}_{AB} = a^{\mathrm{e}}_{AB} - \frac{1}{4r_{\mathrm{opt}}\chi}\tilde{f}_A\tilde{f}_B, \quad \tilde{f}_A = g_A + r_{\mathrm{opt}}f_A. \tag{97}$$

Type (a) singularity of this tensor occurs when $\det(\tilde{a}^{\mathrm{ep}}_{AB}) = 0$. For the example discussed above we determined that $\det(\tilde{a}^{\mathrm{ep}}_{AB}) < 0$ right at onset of plasticity. Thus, for this particular loading condition not a single step in the plastic loading regime is covered by the exclusion condition of Raniecki and Bruhns [36].

To further illustrate the interplay among the various stability criteria, we next consider the following strain-driven load path: $\Delta\epsilon_{11} = -0.005\%$; $\Delta\epsilon_{22} = -0.003\%$; $\Delta\epsilon_{33} = -0.001\%$; $\Delta\gamma_{12} = 2\Delta\epsilon_{12} = +0.002\%$; $\Delta\gamma_{23} = \Delta\gamma_{13} = 0$. This leads to an imposed net volumetric strain increment $\Delta\epsilon_{\mathrm{v}} = -0.006\%$ (compressive) as well as to a rotation of principal axes on plane 1–2. Figure 9 plots the relevant determinants. We observe that nowhere does the determinant of the acoustic tensor cross zero, so this imposed strain path will not trigger a deformation band. We also see that the determinant of the matrix $[a^{\mathrm{ep}}_{AB}]$ for the "in-loading" comparison solid crosses the value zero at step number 62, so the response is expected to bifurcate near this load step. The calculated e-mode has principal jumps $[\![\dot{\epsilon}_A]\!] = \{-0.891, -0.425, -0.160\}$, again normalized to have a unit norm; by definition in Fig. 3 and Box 1, this is a strictly implosive bifurcation mode. Finally, we see that the determinant of the matrix $[\tilde{a}^{\mathrm{ep}}_{AB}]$ crosses the value zero at step number 44, so the exclusion condition covers the plastic regime up until step number 44, i.e., the solution is guaranteed to be stable up until this step number. Tvegaard [42] noted that the lower bounds on the bifurcation load predicted by (96) often appear to be conservative. This seems to be corroborated by Fig. 9 in which the exclusion condition terminates at load step #44, much sooner than when the in-loading comparison solid bifurcates at load step #62.

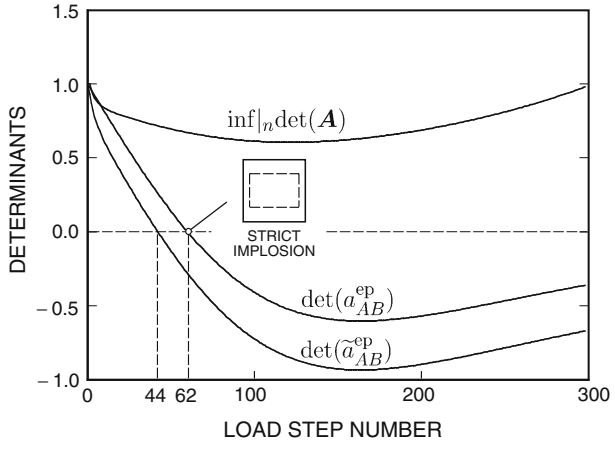

Fig. 9 Simulation of a strictly implosive bifurcation mode, non-associative plasticity case

6 Closure

We have presented conditions for pore collapse instabilities in solids induced by a local bifurcation of solution into non-unique strain rate fields. We have highlighted bifurcation modes as they augment (and complement) current understanding of instabilities associated with deformation banding. The theory was applied to a three-invariant non-associative plasticity model allowing for yielding and plastic flow in compression. Results of the simulations suggest that a deformation band analysis alone is not sufficient to address the loss of uniqueness of solution, and that diffuse pore collapse instabilities may also occur well into the early stage of the solution. A natural extension of the present theory would entail formulation with finite deformation in the presence of pore fluids. This aspect opens an entirely different approach to addressing the problem of liquefaction instability in granular soils, for example; work on this aspect is currently in progress. Finally, we note that in shear band analysis finite element solutions are now being pursued into the post-localization regime utilizing some form of strain enhancements to capture localized deformation [6, 8, 11, 37]. It appears that pore collapse instabilities can also be treated at post-bifurcation using a similar strategy provided that one utilizes an appropriate e-mode to construct the enhanced strain.

Acknowledgments The author is very grateful to two anonymous reviewers for their expert reviews, and to graduate student Pablo Sanz for rendering the three-dimensional solid figures presented in this paper. This work is supported by National Science Foundation Grant Nos. CMS-0201317 and CMS-0324674, and US Department of Energy Grant No. DE-FG02-03ER15454.

References

1. Antonellini MA, Aydin A, Pollard DD (1994) Microstructure of deformation bands in porous sandstones at Arches National Park, Utah. J Struct Geol 16:941–959
2. Aydin A, Borja RI, Eichnubl P (2006) Geological and mathematical framework for failure modes in granular rock. J Struct Geol 28:83–98
3. Bigoni D (1999) Bifurcation and instability of non-associative elastoplastic solids. In: Petryk H (Coordinator) CISM Lecture notes on the course: Material instabilities in elastic and plastic solids, Udine, Sept. 13–17

4. Bigoni D, Hueckel T (1991) Uniqueness and localization—I. Associative and non-associative plasticity. Int J Solids Struct 28:197–213
5. Bigoni D, Zaccaria D (1992) Loss of strong ellipticity in non-associative elastoplasticity. J Mech Phys Solids 40:1313–1331
6. Borja RI (2000) A finite element model for strain localization analysis of strongly discontinuous fields based on standard Galerkin approximations. Comput Methods Appl Mech Eng 190:1529–1549
7. Borja RI (2002) Bifurcation of elastoplastic solids to shear band mode at finite strain. Comput Methods Appl Mech Eng 191:5287–5314
8. Borja RI (2002) Finite element simulation of strain localization with large deformation: capturing strong discontinuity using a Petrov–Galerkin multiscale formulation. Comput Methods Appl Mech Eng 191:2949–2978
9. Borja RI (2004) Computational modeling of deformation bands in granular media, II: Numerical simulations. Comput Methods Appl Mech Eng 193:2699–2718
10. Borja RI, Aydin A (2004) Computational modeling of deformation bands in granular media, I: Geological and mathematical framework. Comput Methods Appl Mech Eng 193:2667–2698
11. Borja RI, Regueiro RA (2001) Strain localization of frictional materials exhibiting displacement jumps. Comput Methods Appl Mech Eng 190:2555–2580
12. Borja RI, Sama KM, Sanz PF (2003) On the numerical integration of three-invariant elastoplastic constitutive models. Comput Methods Appl Mech Eng 192:1227–1258
13. Borre G, Maier G (1989) On linear versus nonlinear flow rules in strain localization analysis. Meccanica 24:36–41
14. Chambon R (2005) Some theoretical results about second order work, uniqueness, existence and controllability independent of the constitutive equation. J Eng Math 52:53–61
15. Chambon R, Crochepeyre S, Desrues J (2000) Localization criteria for non-linear constitutive equations of geomaterials. Mech Cohes Frict Mater 5:61–82
16. Chau K-T, Rudnicki JW (1990) Bifurcations of compressible pressure-sensitive materials in plane strain tension and compression. J Mech Phys Solids 38:875–898
17. Crisfield MA (1997) Non-linear finite element analysis of solids and structures, Vol 2. Wiley, Chichester
18. Hadamard J (1903) Lecons sur la Propagation des Ondes. Herman et fil, Paris
19. Hill R (1958) A general theory of uniqueness and stability in elastic-plastic solids. J Mech Phys Solids 6:236–249
20. Hill R (1978) Aspect of invariance in solid mechanics. Adv Appl Mech 18:1–75
21. van den Hoek PJ, Kooijman AP, de Bree P, Kenter CJ, Zheng Z, Khodaverdian M (2000) Horizontal-wellbore stability and sand production in weakly consolidated sandstones. SPE Drill Complet 15(4):274–283
22. Issen KA, Rudnicki JW (2000) Conditions for compaction bands in porous rock. J Geophys Res 105:21529–21536
23. Kim MK, Lade PV (1988) Single hardening constitutive model for frictional materials I. Plastic potential function. Comput Geotech 5:307–324
24. Lade PV (1992) Static instability and liquefaction of loose fine sandy slopes. J Geotech Eng ASCE 118:51–71
25. Lade PV, Kim MK (1988) Single hardening constitutive model for frictional materials II. Yield criterion and plastic work contours. Comput Geotech 6:13–29
26. Lade PV, Kim MK (1988) Single hardening constitutive model for frictional materials III. Comparisons with experimental data. Comput Geotech 6:31–47
27. Marsden JE, Hughes TJR (1983) Mathematical foundations of elasticity. Prentice-Hall, Englewood Cliffs
28. Morita N, Whitfill DL, Massie I, Knudsen TW (1989) Realistic sand-production prediction: numerical approach. SPE Prod Eng Trans AIME 287:15–24
29. Morita N, Whitfill DL, Fedde OP, Lovik TH (1989) Parametric study of sand-production prediction: analytical approach. SPE Prod Eng Trans AIME 287:25–33
30. Murray RM, Li Z, Sastry SS (1994) A mathematical introduction to robotic manipulation. CRC Press, Boca Raton
31. Nova R (1994) Controllability of the incremental response of soil specimens subjected to arbitrary loading programmes. J Mech Behav Mater 5:221–243
32. Ogden RW (1984) Non-linear elastic deformations. Ellis Horwood Ltd., Chichester
33. Olsson WA (1999) Theoretical and experimental investigation of compaction bands in porous rock. J Geophys Res 104(B4):7219–7228
34. Olsson WA (2001) Quasistatic propagation of compaction fronts in porous rock. Mech Mater 33:659–668
35. Olsson WA, Holcomb DJ (2000) Compaction localization in porous rock. Geophys Res Lett 27:3537–3540
36. Raniecki B, Bruhns OT (1981) Bounds to bifurcation stresses in solids with non-associated plastic flow law at finite strain. J Mech Phys Solids 29:153–172
37. Regueiro RA, Borja RI (2001) Plane strain finite element analysis of pressure-sensitive plasticity with strong discontinuity. Int J Solids Struct 38:3647–3672
38. Rice JR (1977) The localization of plastic deformation. In: Koiter WT (ed) Theoretical and applied mechanics. North-Holland, Amsterdam, pp 207–220
39. Rice JR, Rudnicki JW (1980) A note on some features of the theory of localization of deformation. Int J Solids Struct 16:597–605
40. Rudnicki JW, Rice JR (1975) Conditions for the localization of deformation in pressure-sensitive dilatant materials. J Mech Phys Solids 23:371–394
41. Thomas TY (1961) Plastic flow and fracture of solids. Academic, New York
42. Tvergaard V (1982) Influence of void nucleation on ductile shear fracture at a free surface. J Mech Phys Solids 30:399–425
43. Vardoulakis I, Goldscheider M, Gudehus G (1978) Formation of shear bands in sand bodies as a bifurcation problem. Int J Numer Anal Methods Geomech 2:99–128